



# HHS Public Access

Author manuscript

*J Comp Neurol.* Author manuscript; available in PMC 2018 February 01.

Published in final edited form as:

*J Comp Neurol.* 2017 February 01; 525(2): 271–290. doi:10.1002/cne.24059.

## Immunocytochemical Organization and Sour Taste Activation in the Rostral Nuc. Solitary Tract of Mice

Jennifer M. Stratford<sup>1</sup>, John A. Thompson<sup>2</sup>, and Thomas E. Finger<sup>1,3</sup>

<sup>1</sup>Rocky Mountain Taste & Smell Center, Department of Cell and Developmental Biology, University of Colorado School of Medicine, Aurora, CO USA

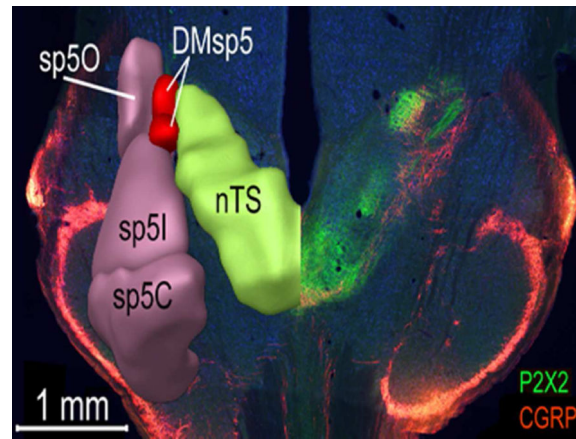
<sup>2</sup>Department of Neurosurgery, University of Colorado School of Medicine, Aurora, CO USA

<sup>3</sup>Program in Neuroscience, University of Colorado Anschutz Medical Campus, Aurora, CO USA

### Abstract

Sensory inputs from the oropharynx terminate in both the trigeminal brainstem complex and the rostral part of the nucleus of the solitary tract (nTS). Taste information is conveyed via the facial and glossopharyngeal nerves while general mucosal innervation is carried by the trigeminal and glossopharyngeal nerves. In contrast, the caudal nTS receives general visceral information largely from the vagus nerve. Although the caudal nTS shows clear morphological and molecularly delimited subdivisions, the rostral part does not. Thus, linking taste-induced patterns of activity to morphological subdivisions in the nTS is challenging. To test whether molecularly-defined features of the rostral nTS correlate with patterns of taste-induced activity, we combined immunohistochemistry for markers of various visceral afferent and efferent systems with c-Fos-based activity maps generated by stimulation with a sour tastant, 30mM citric acid. We further dissociated taste-related activity from activity arising from acid-sensitive general mucosal innervation by comparing acid-evoked c-Fos in wildtype and “taste blind”, P2X<sub>2</sub>/P2X<sub>3</sub> double knockout (P2X-dblKO) mice. In wildtype mice, citric acid stimulation evoked significant c-Fos activation in the central part of the rostral nTS – activity that was largely absent in the P2X-dblKO mice. P2X-dblKO mice, like wildtype mice, did exhibit acid-induced c-Fos activity in the dorsomedial trigeminal brainstem nucleus situated laterally adjacent to the rostral nTS. This dorsomedial nucleus also showed substantial innervation by trigeminal nerve fibers immunoreactive for CGRP, a marker for polymodal nociceptors suggesting that trigeminal general mucosal innervation carries information about acids in the oral cavity.

### Graphical Abstract



Responses to sour (acid) stimuli occur not only within taste-responsive regions of the nucleus of the solitary tract (nTS), highlighted by P2X<sub>2</sub>-immunoreactive fibers (green) but also within the dorsomedial nucleus of the brainstem trigeminal complex (DMSp5), which receives input from polymodal nociceptors of the oral cavity, marked by CGRP-immunoreactivity (red).

### Keywords

CGRP; acid; c-Fos; trigeminal; esophagus; oropharynx; RRID: AB\_2040054; RRID: AB\_572253; RRID: AB\_518351; RRID: AB\_518147; RRID: AB\_2314042

### Introduction

Sensations from the oropharynx are key in distinguishing foods from potential toxins. This region has a complex innervation involving cranial nerves mediating taste sensations as well as those providing general innervation of the mucosa. The gustatory nerves, including the facial and glossopharyngeal nerves, innervate taste buds of the oral cavity while the superior laryngeal branch of the vagus nerves innervates taste buds of the larynx (Dickman and Smith, 1988). The gustatory nerves convey sensations of taste, i.e. sweet, umami, bitter, salty and sour, the last of these being triggered by low pH. But acidity is reported not only by taste nerves, but also by pH-sensitive components of the general mucosal innervation provided by trigeminal, glossopharyngeal and vagus nerves. The redundancy in acid detection is evidenced by the ability of mice that lack the sense of taste to nonetheless detect and avoid acidic solutions (Hallock *et al.*, 2009; Ohkuri *et al.*, 2012).

Sensory information from the orosensory nerves terminates within the dorsal medulla in the nucleus of the solitary tract and laterally adjacent medullary trigeminal complex. The nucleus of the solitary tract (nTS) is the primary sensory nucleus for the visceral senses including taste and related oral sensations as well as general visceral inputs from the respiratory and digestive systems. Nerves serving the functionally different visceral modalities, e.g. cardiac, gastric, respiratory, each terminate in a restricted subnucleus of the caudal solitary complex (Katz and Karten, 1983; Altschuler *et al.*, 1989), while taste and oral functions target the rostral two-thirds of the nuclear complex (Hanamori and Smith, 1986; Bradley, 2007; Whitehead and Finger, 2008; Felizardo *et al.*, 2009; Corson *et al.*, 2012). The

nTS is readily identified in transverse sections through the medulla of all amniote vertebrates by the distinctive absence of myelin staining in that area. Despite this common overall appearance, the exact boundaries and subdivisions of the nucleus are difficult to delineate without recourse to hodological or histochemical methods. Although detailed cytochemical studies reveal significant correlations between neuropeptide distribution and functional compartments of the caudal nTS in a variety of species (Altschuler *et al.*, 1989; Berk *et al.*, 1993; Rogers and McCann, 1993; Wank and Neuhuber, 2001), little data exist regarding cytochemical heterogeneity of rostral nTS, i.e. the area implicated in taste-related food acceptance or rejection. In the present report, we consider the anatomical relationships of several feeding-related peptide systems and primary afferent systems with the rostral and central nTS and adjacent trigeminal nuclei of mouse and compare these to the distribution of neurons activated by oral stimulation with acidic solutions.

The diversity of sensory and motor inputs into the rostral and intermediate nTS is paralleled by a likewise diverse population of nTS cells that utilize numerous neurotransmitters for communication, including glutamate, GABA, acetylcholine and substance P (Davis, 1993; Davis and Smith, 1997; King, 2003; Uteshev and Smith, 2006; Wang and Bradley, 2010; Corson and Erisir, 2013). This cellular heterogeneity in the rostral and intermediate nTS makes delineation of functional nTS subdivisions difficult. In the past, researchers have used regional differences in soma sizes or patterns of myelin staining to delineate nTS subregions (Whitehead, 1988; Whitehead, 1990; Halsell *et al.*, 1996; Corson *et al.*, 2012; Ganchrow *et al.*, 2014). Although useful, adoption of these techniques has been hampered by inconsistencies in the demarcation of nTS boundaries that results from using these two techniques-especially with respect to the lateral and ventral borders of the rostral nTS (Fig. 1). Moreover, defining boundaries of nTS subregions is somewhat subjective, especially for the brainstem of mice. Thus, the creation of a standardized, agreed-upon set of criteria for the boundaries of the nTS remains elusive.

To address this issue, we utilized ‘chemical dissection,’ as successfully used by others previously, to delineate functional boundaries of the nTS and adjacent nuclei (Herbert and Saper, 1990; Berk *et al.*, 1993). To do this, we first systemically compared the boundaries of the nTS as defined using either a nuclear Nissl stain or a fluorescent myelin stain; then mapped the spatial distribution of neuropeptides and neurotransmitters involved in primary afferent or efferent functions of the nTS and surrounding regions, including the purinergic receptor, P2X<sub>2</sub>, (in afferents that innervate the oral cavity; Bartel, 2012; Breza and Travers, 2016), acetylcholine (in motor nuclei including the dorsal motor nucleus of the vagus), the orexigenic peptides: neuropeptide Y (NPY) (Chen *et al.*, 2012) and galanin (in limited primary afferents innervating different visceral organs) (Finley *et al.*, 1995), and particularly, calcitonin gene-related peptide (CGRP) in polymodal nociceptors of the trigeminal and glossopharyngeal nerves innervating the oropharynx, as well as in a variety of vagal afferents that innervate various visceral organs, including the esophagus (Sykes *et al.*, 1994; Sugimoto *et al.*, 1997; Wank and Neuhuber, 2001; Hayakawa *et al.*, 2009; Ma *et al.*, 2011). These CGRP-positive fibers were of particular interest in that many of these neurons also express the acid-responsive Trp channels, TrpA1 or TrpV1 (Bae *et al.*, 2004; Usoskin *et al.*, 2015). We could assess the contribution of these peptidergic nociceptors in responses to

acidic tastants by comparing the distribution of acid-activated, c-Fos positive, cells in wildtype mice to those lacking the sense of taste (P2X<sub>2</sub>/P2X<sub>3</sub> double KO mice).

## Methods

### Animals

Adult C57BL6/J mice purchased from The Jackson Laboratory (Bar Harbor, MN) were used for all immunohistochemical staining except as noted below (Table 1). For visualization of cholinergic neurons, we relied on a BAC transgenic line in which the promoter for choline acetyltransferase, the rate-limiting enzyme for acetylcholine, drives expression of tau-coupled green fluorescent protein (GFP) driven by a choline acetyltransferase promoter (ChAT-tauGFP; RRID: MGI: 5605267; Grybko *et al.*, 2011).

We also utilized P2X<sub>2</sub>/P2X<sub>3</sub> double knockout mice (P2rx2<sup>tm1Ckn</sup> × P2rx3<sup>tm1Ckn</sup>; RRID: MGI\_2687353; P2X-dbl-KO, n = 8), which lack a functional sense of taste (Finger *et al.*, 2005; Eddy *et al.*, 2009), and their background-matched controls (P2X WT; n = 7). Both of these lines are on a mixed Ola-C57B16 background. Because of difficulties in breeding the P2X-dbl KO mice, the knockouts and controls are bred separately, but the knockouts are backcrossed into the WT control lines every 2 generations to maintain genotype similarity across lines.

All animal procedures were performed in accordance with NIH guidelines and were approved by the Institutional Animal Care and Use Committee at the University of Colorado Denver School of Medicine.

### Citric Acid Stimulation for c-Fos via Intraoral Cannula

**Cannulae implantation**—Acid-evoked neuronal activation was assessed in both WT and P2X-dblKO mice. Bilateral intraoral cannulae were implanted into experimental animals as described previously (Stratford and Thompson, 2016). Briefly, mice were anesthetized with an intramuscular (IM) injection of a combination of medetomidine hydrochloride (Domitor®; 0.4 mg/kg; Pfizer, Helsinki, Finland) and ketamine hydrochloride (40 mg/kg; Bioniche Pharma, Lake Forest, IL). Intraoral cannulae were inserted via a midline incision immediately caudal to the pinnae. Then a sterile, 1.5 inch, stainless steel hypodermic needle (19 gauge; Hamilton, Reno, NV) was inserted in the back of the neck and guided subcutaneously into the oral cavity, lateral to the first maxillary molar.

A polyethylene tube (50 gauge; Becton Dickinson and Company, Sparks, MD) was flared using a cautery iron, and then fed through a small, flat # 0 nylon washer (Product Components Corporation; Martinez, CA) and then through the tip of the hypodermic needle. The needle was then withdrawn, leaving the polyethylene cannula and washer in place in the rear of the oral cavity. The wound was then closed with Dexon II 6.0 mm suture (Syneture, Norwalk, CT), and a second nylon washer secured the loose end of the tubing against the skin on the back of the neck. The remaining tubing was flared by heating the exposed tubing with a cautery and a blunt 1" hypodermic needle (25 gauge; McKesson, San Francisco, CA) was secured to the loose end of the tubing and served as a metal fistula. Animals were allowed to recover for 5 days prior to training (see below).

**Cannula training and c-Fos Stimulation**—Fluids were delivered into intraoral cannulae via a 5 cc syringe (Becton Dickinson and Company, Sparks, MD) connected to a syringe pump (Model R99-E, Razel Scientific Instruments, St. Albans, VT). To acclimate mice to stimulation procedures, all animals were placed on 23 h/day water restriction schedule three days prior to stimulation, and received 3 ml of dH<sub>2</sub>O infused over the course of 30 min each day into one of two intraoral cannulae at a flow rate of 0.10 ml/ min. As in previous studies (Stratford and Thompson, 2016), on the stimulation day, 3 ml of either deionized water (control; n = 2 for both P2X WT and P2X-dblKO) or 30 mM citric acid (n = 5 for P2X WT and n = 6 for P2X-dblKO) was infused into a single intraoral cannula at a constant flow rate (0.10 ml/ min) over the course of 30 min. In previous experiments (Eylam *et al.*, 2005; Finger *et al.*, 2005; Hallock *et al.*, 2009), 30mM citric acid is non-aversive or only moderately aversive to the mice in brief access (lickometer) taste tests but strongly avoided in longer-term consumption (2-bottle preference) tests. Animals exposed to the stimulus were left undisturbed for 45 min prior to perfusion.

**c-Fos Immunohistochemistry**—Forty-five min following taste stimulation, animals were deeply anesthetized with Fatal-Plus<sup>®</sup> (50 mg/kg intraperitoneally; MWI, Boise, ID) or pentobarbital (i.p. injection 100mg/kg in saline), then perfused transcardially with saline (0.9% sodium chloride) followed by 4% paraformaldehyde (PFA) in 0.1M phosphate buffer, pH 7.2–7.4 (PB). The brains were post fixed for three hours at room temperature, then cryoprotected overnight in 20% sucrose in PB at 4°C. Brainstems were blocked in the transverse plane just anterior to the cerebellum. The olfactory bulbs were also sectioned and used as a positive control for brains processed for c-Fos immunohistochemistry. After cryoprotection, tissues were embedded in OCT (Optimal Cutting Temperature compound Fisher Scientific, Pittsburgh, PA), frozen, and sectioned at 40 µm using a Leica cryostat. Free-floating sections were collected in 0.9 % NaCl in PB (PBS). Sections were washed three times in PBS, then transferred to a blocking medium consisting of 2% normal donkey serum (NDS, Jackson ImmunoResearch, West Grove, PA; RRID: AB\_2337258) diluted in antibody medium (AB medium; 0.3% triton, 0.15 M sodium chloride, and 1% bovine serum albumin in PB) for one hour at room temperature.

### General Immunohistochemistry Methods

All staining was carried out using standard immunohistochemical procedures. Briefly, primary antisera (Table 2) were diluted in AB medium and incubated between 1 and 2 days (see details below) at 4°C. Then, 3 10 min. rinses in 0.1M PBS preceded a 2h incubation in secondary antibodies (see below). All tissue was counterstained with NeuroTrace Nissl stain 640/680 (1:100; Thermo Fisher Scientific; Cat# N21483; Lot #'s 572097 and 927003; RRID: AB\_2572212) or FluoroMyelin (1:50; Thermo Fisher Scientific; Cat# F34652; Lot # 1314308; RRID: AB\_2572213), which was included in the AB medium during incubation in secondary antisera, except where noted. Following an additional three 0.1M PBS washes, free floating tissue sections were mounted onto Superfrost Plus slides (Fisher Scientific, Pittsburgh, PA), and then cover-slipped using Fluoromount – G (Southern Biotech, Birmingham, Alabama). Endogenous ChAT GFP was visualized without the use of a primary antibody.

### **P2X<sub>2</sub>/ChAT Single Label Immunohistochemistry**

For P2X<sub>2</sub> staining, tissue was incubated in primary antiserum (Alomone Labs; Cat# APR-003; Lot# AN-08; RRID: AB\_2040054; Table 2) for two nights at 4°C diluted in AB medium. Following three 0.1M PBS washes, the tissue was incubated for two-hours in AlexaFluor 488 1:400 (donkey anti-rabbit, Molecular Probes Cat# A21206; Lot# 913921; RRID: AB\_141708).

### **Double Label Immunohistochemistry with Different Host Species (P2X<sub>2</sub>/ Galanin)**

Primary antisera for P2X<sub>2</sub> and Galanin were applied simultaneously (Alomone Labs Cat# APR-003; Lot# AN-08; RRID: AB\_2040054; Table 2) for 2 nights at 4°C. The sections were rinsed in 0.1M PBS and incubated with Alexa Fluor 568 (donkey anti-rabbit, Thermo Fisher Scientific; Cat# A10042; Lot #'s 790344 and 685232; RRID: AB\_11180183, Invitrogen, Carlsbad, CA) and 488 (donkey anti-guinea pig, Jackson ImmunoResearch Labs; Cat# 706-545-148; Lot# 105625; RRID: AB\_2340472) secondary antibodies diluted 1:400 in AB media.

### **Immunohistochemistry with Same Host Species Using Zenon Kit (P2X<sub>2</sub>/CGRP; P2X<sub>2</sub>/ NPY)**

Sections were first incubated in antiserum to either NPY (Bachem; Cat# T-5036.0050; Lot# 1112001 RRID: AB\_518351) or CGRP (Bachem; Cat# T-4032.0050; Lot# A07725; RRID: AB\_518147) (Table 2) for 2 nights at 4°C. Then, tissue was rinsed 3 times in 0.1M PBS, followed by a 2 hour incubation at room temperature with a Rhodamine Red-X Fab Fragment (donkey anti-rabbit, Jackson ImmunoResearch Labs; Cat# 711-297-003; Lot# 103577; RRID:AB\_2340615) secondary antibody diluted 1:100 in AB medium. Then sections were rinsed in 0.1M PBS 2 times and in PBST (PBS containing 0.4% triton) once. The Zenon Labeling Kit (Alexa Fluor 488 rabbit kit, Thermo Fisher Scientific; Cat: Z25302; Lot # 695640; RRID: AB\_2572214) was prepared just prior to use as follows. 1 µg of P2X<sub>2</sub> antibody was diluted in 5 µl of Zenon labeling reagent, spun down in a centrifuge, and left undisturbed for 5 minutes at room temperature. 5 µl of blocking reagent was then added to the above solution, spun down and left undisturbed for 5 minutes to create the Zenon complex. The Zenon complex was diluted to a final concentration of 1:100 using PBST. Brainstem sections were then incubated with this diluted P2X<sub>2</sub> antibody for 75 minutes. After incubation, sections were rinsed in PBST and then post fixed for 15 minutes in 4% PFA in 0.1M PB.

### **Immunohistochemistry with Same Host Species Using Unlabeled FAB fragment (citric acid-evoked c-Fos/ CGRP)**

Because preliminary results indicated that c-Fos protein immunoreactivity could not be detected reliably using a Zenon kit (see methods above), citric acid-evoked c-Fos/ CGRP double-labeling was done using an alternative method. Sections were first incubated in c-Fos antisera (Table 2) for 2 nights at 4°C. Then, tissue was rinsed 3 times in 0.1M PBS, followed by a 2 hour incubation at room temperature with a Rhodamine Red-X Fab Fragment (donkey anti-rabbit, Jackson ImmunoResearch Labs; Cat# 711-297-003; Lot# 112848; RRID:AB\_2340615) secondary antibody diluted 1:100 in AB medium. Sections were then rinsed in 0.1M PBS 3 times and incubated with a donkey anti-rabbit unlabeled FAB

fragment (1:50; Jackson ImmunoResearch Labs; Cat# 711-007-003; Lot# 106860; RRID: AB\_2340587) for 2 nights at 4°C. Incubation with a donkey anti-rabbit unlabeled FAB fragment blocks any exposed, rabbit-specific IgG epitopes on the c-Fos antibody, preventing non-specific labeling of a second rabbit-specific antibody. Then, tissue was rinsed 3 times in 0.1M PBS, followed by a 2 hour incubation at room temperature with an Alexa Fluor 488 (donkey anti-rabbit, Molecular Probes Cat# A21206; Lot# 1378892; RRID: AB\_141708) secondary antibody diluted 1:400 in AB media. A lack of apparent double-label cells or fibers indicates the specificity of this method.

### Representative Levels of the Nucleus of the Solitary Tract and c-Fos cell counting

To thoroughly characterize P2X<sub>2</sub>/neuropeptide distribution, as well as citric-acid evoked c-Fos activity, throughout the rostral and intermediate parts of the nTS, we divided the nTS into 9 rostral-caudal levels, as described in detail previously (Stratford and Finger, 2011). Briefly, the rostrocaudal levels are designated as rostral (r1 – r4) and intermediate (i1 – i5); situated respectively at –6.36, –6.48, –6.72, –6.96, –7.08, –7.20, –7.32, –7.48, and –7.56 from bregma; see Fig. 1). For each level, we further divided the region of the nTS into 6 subfields: lateral, central (middle), and medial for dorsal and ventral tiers.

To quantify the number of c-Fos positive cells, the red (c-Fos) color channel in each image was filtered based on a stringent threshold (mean + 2 standard deviations of background pixel intensity level), and then the red color channel was converted to a binary BW image using *ImageBWconvertGUI*—a custom-made program running in the 2013a Matlab Computing Environment with the Image Processing Toolbox (The MathWorks, Natick, MA; RRID: SCR\_001622; program available on Github; RRID: SCR\_002630:<https://github.com/neuropil/ImageBWconvert/>). This resulted in filtered binary black and white images of c-Fos staining > 2 standard deviations of background staining for each animal. Then, the number of c-Fos positive cells was quantified using the cell counter plug-in in ImageJ (version 1.47, Bethesda, MD; RRID: SCR\_003070). Cases were counted only when substantial Fos-LI was observed in the olfactory bulb, as c-Fos expression is robust in the olfactory bulb in all animals (Guthrie *et al.*, 1993).

### Imaging of P2X<sub>2</sub>/ Neuropeptide/ Nissl Sections

Images of P2X<sub>2</sub>/neuropeptide/Nissl stained brainstem sections were photographed at 10X magnification using Q Capture software (RRID: SCR\_014432; QImaging, Surrey, BC, Canada) with a monochrome Q-imaging camera on an Olympus BX41TF microscope. Image acquisition exposure times for each fluorophore were the same for each set of P2X<sub>2</sub>/neuropeptide/ Nissl stains.

### Imaging of P2X<sub>2</sub>/ Neuropeptide/ FluoroMyelin Sections and as Citric Acid-Evoked C-Fos/ CGRP Cases

Whole slide images sections were photographed using Surveyor by Objective Imaging software (RRID: SCR\_014433; Cambridge, UK; [http://www.objectiveimaging.com/Surveyor/OI\\_Turboscan.htm](http://www.objectiveimaging.com/Surveyor/OI_Turboscan.htm)) with a monochrome Leica DFC 365FX camera on a Leica DM6000B microscope. For each fluorophore, a series of 10X images, aligned in a grid, were obtained using the Multiscan setting. Each channel (FITC, Texas Red and Cy-5) was

obtained sequentially and merged together. Images were then stitched together in real time using the best focus algorithm in the Surveyor software, which yielded a mosaic image of the whole microscope slide. Then images of whole brain sections were exported as single images using the Region of Interest selection tool in Surveyor. As done with P2X<sub>2</sub>/neuropeptide/Nissl sections above, exposure times were consistent within each set of stains.

### Spatial Neuropeptide Mapping

Visualization of the spatial distribution within each nTS section of P2X<sub>2</sub> and each neuropeptide was done using PixelIntensity- a custom image analysis program running in the 2012a version of the Matlab Computing Environment (RRID:SCR\_001622; The MathWorks, Natick, MA; <https://github.com/neuropil/HeatMappingProgram>). Background pixel intensity was calculated for each channel separately using a (150×150 pixel) square polygon averaged across all 9 representative nTS sections. To quantify pixel intensity in regions of interest, a polygon was drawn around the region of interest (i.e. nTS) and neuropeptide label was defined based on a stringent threshold (mean + 2 standard deviations (S.D.) of background pixel intensity level). Then the pixels that met this 2 + S.D. criteria were used to create a 2-D spatial distribution map for each neuropeptide.

### Post Image Acquisition Processing

All images used to map the spatial distribution of neuropeptides were unaltered prior to being analyzed with the PixelIntensity program (see above). Brightness and contrast of all photographs shown as representative sections in all figures were optimized in Adobe Photoshop CS5 (RRID: SCR\_014199; San Jose, CA) using the levels and hue tools. For use in all figures, spatial distribution plots generated by the PixelIntensity program were first saved as .tiff images within MATLAB. Then these images were converted into binary images within Adobe Photoshop CS6 using the 'mode' and 'levels' tools. Finally, each binary density image was then false colored (magenta or green) and pairs of P2X<sub>2</sub>/neuropeptide plots (e.g. P2X<sub>2</sub>/ NPY, P2X<sub>2</sub>/ ChAT, etc.) were combined into a single image.

### Characterization of Primary Antibodies

**Purinergic P2X<sub>2</sub> Receptor**—The ionotropic ATP receptor P2X<sub>2</sub> was used as a marker of primary afferent gustatory fibers (Ganchrow *et al.*, 2014). The antibody was produced in rabbits against the C-terminus of the rat P2X<sub>2</sub> sequence. A western blot revealed a single 80kD band from PC12 cell lysates. No P2X<sub>2</sub> staining was observed by immunohistochemistry in a mouse where P2X<sub>2</sub> was genetically deleted (Finger *et al.*, 2005).

**Neuropeptide Y (NPY)**—The manufacturer analyzed this antibody by using the biotin-streptavidin/ horseradish peroxidases (HRP) detection method on rat brain tissue. All staining was blocked by preabsorption of the diluted antiserum with excess NPY (10<sup>-6</sup> M). Cross-reactivity experiments in which diluted NPY antiserum was absorbed with excess (10<sup>-6</sup> M) peptide YY, avian pancreatic polypeptide, B-endorphin, vasoactive intestinal peptide, cholecystokinin, or somatostatin showed no effect in blocking the intensity of staining (Immunostar Data Sheet).

**Galanin**—The polyclonal antibody recognizes porcine galanin determined by radioimmunoassay (Peninsula data sheet). The antibody stains similarly to the polyclonal rabbit-anti galanin antibody that cross-reacts with rat galanin, and not Secretin, VIP, Neuropeptide-Y, Substance-P, or Insulin determined by radioimmunoassay (Peninsula Labs data sheet, cat. no.T-4330). As in Klein *et al.*, 2006 preabsorption with synthetic 10 µg porcine/rat galanin (1450; Tocris, Minneapolis, MN) eliminated staining in the mouse brainstem.

**Calcitonin Gene-Related Peptide (α-CGRP)**—The antiserum recognizes canine, rat, and mouse α-CGRP as determined by radioimmunoassay (Peninsula data sheet). A Western blot revealed a 4 kDa band in the mouse trigeminal ganglion and preabsorption with CGRP eliminated staining on the mouse trigeminal ganglion (Kosaras *et al.*, 2009). The antibody staining was in agreement with that shown for the mouse trigeminal ganglion (Kosaras *et al.*, 2009).

**c-Fos**—The polyclonal antibody recognizes residues 4–17 of the human c-Fos protein (Calbiochem data sheet). This antiserum stains a single band at ~50 – 55 kDa as observed by Western Blot analysis of Fibroblast-like BHK 21 C13 cells (Archer *et al.*, 1999). Moreover, omission of rabbit anti-c-Fos antibody resulted in no labeled cells (data not shown; Ingham *et al.*, 2009; Kelsch *et al.*, 2012).

### Statistical Analysis for c-Fos Activity

To determine acid-specific c-Fos activation, for each subdivision of the nTS or the dorsomedial nucleus of the descending trigeminal complex (DMSp5), counts of c-Fos positive cells following water stimulation were subtracted from counts following acid stimulation. This yielded an index of the number of cells specifically activated by oral exposure to acid. c-Fos cell counting data presented in the results and in Fig. 12 are presented as group means ± SD. Data were analyzed using appropriate two-way ANOVAs (Statistica; RRID:SCR\_014213; StatSoft, Tulsa, OK). Tukey's honest significant difference tests were used to assess statistically significant ( $p < 0.05$ ) main effects or interactions.

## Results

The nTS can be readily identified as a longitudinally oriented column of closely-spaced, small neurons (~ 9 – 10 µm) situated in the dorsal medulla and extending the length of the rostral medulla reaching caudally to the level of the area postrema. The rostral end of the nTS lies just medial to the dorsomedial nucleus of the descending trigeminal complex at the level of entrance of the facial nerve, but moves medially as the nTS approaches the area postrema. Although the nTS can be seen easily in relatively low magnification images of the medulla, its exact boundaries are indistinct.

Conventionally, the nucleus is recognized by its appearance in Nissl-stained preparations, although some recent works (e.g. Corson *et al.*, 2012) have relied on myelin staining to demarcate the nucleus since it contains relatively few myelinated fibers. Unfortunately, comparison of the boundaries drawn by these two methods appear to differ substantially (Figs. 1 and 2). Furthermore, the nTS often is divided into subnuclei based on differences in

cell staining and packing density in Nissl-stained preparations (e.g. Ganchrow *et al.*, 2014), but we have found it difficult to discern distinct boundaries between the various subnuclei based solely on Nissl staining characteristics in mice (Fig. 2). The different component subnuclei of the caudal part of the nTS, which subserve different viscerosensory modalities, tend to be more cytologically distinct than components of the rostral nTS, which is more devoted to taste and orosensory functions. In this work, we focus on the rostral, gustatory part of the nTS in an attempt to delineate clear boundaries and subdivisions based on objective histochemical and immunocytochemical staining characteristics.

### **P2X<sub>2</sub> immunoreactivity**

Primary gustatory afferent fibers, like many other visceral afferent fiber systems, express high levels of staining for the purinoceptors P2X<sub>2</sub> and P2X<sub>3</sub> (Bartel, 2012; Ganchrow *et al.*, 2014). Furthermore, P2X<sub>2</sub> and P2X<sub>3</sub> staining almost entirely overlaps the field of termination of primary gustatory afferent fibers (Bartel, 2012; Ganchrow *et al.*, 2014; Breza and Travers, 2016). Accordingly, we used staining for the P2X<sub>2</sub> subunit as a surrogate for the incoming viscerosensory and gustatory primary afferents. Fascicles of immunoreactive fibers penetrate the rostral medulla with the facial nerve root, pass through the spinal trigeminal complex and swing laterally along the dorsal margin of the nTS. Starting at the rostral tip of the nTS, these P2X<sub>2</sub><sup>+</sup> fibers give rise to a terminal field in the dorsocentral region of the nTS (Figs. 3, 4, 5, and 7; green; see supplementary figures S1 – S4 for P2X<sub>2</sub><sup>+</sup> fiber distribution across all nine nTS levels), roughly corresponding to the boundaries of the rostralateral (RL) and rostromedial (RM) subnuclei as defined by others (e.g. Ganchrow *et al.*, 2014). At the level of entrance of the glossopharyngeal nerve, additional P2X<sub>2</sub><sup>+</sup> fiber fascicles enter the lateral edge of the medulla, penetrate the spinal trigeminal complex and continue medially to run along the dorsal margin of the nTS apparently contributing to the terminal plexus within the dorsocentral regions of the nTS including but not limited to the Ce (Central) nucleus described by Ganchrow *et al.* (2014). Within the intermediate nTS (i1 – i5), P2X<sub>2</sub> terminal field staining expands medially and somewhat ventrally to cover much of the medial two-thirds of the nTS (Figs. 3 – 5 and 7; S1 – S4) but apparently excluding the M (medial) subnucleus of Ganchrow *et al.*, (2014). Based on previous studies (Corson *et al.*, 2012; Breza and Travers, 2016), this strongly positive P2X<sub>2</sub><sup>+</sup> terminal field appears coincident with the distribution of gustatory and primary viscerosensory afferents of the facial, glossopharyngeal and vagus nerves.

### **Choline Acetyltransferase (ChAT)**

Just as we rely on P2X<sub>2</sub> labeling to be largely coincident with the primary viscerosensory afferent fiber systems, we employed staining for ChAT-driven tauGFP as a surrogate for visceral efferent systems (while recognizing that other sources of ChAT exist). ChAT-GFP labeling occurs predominantly within brainstem motor nuclei throughout the entire medulla, as described previously (Grybko *et al.*, 2011). In particular, dense ChAT-GFP label is present in cell bodies of the DMX adjacent to the rostral nTS (r3 – r4; Figs. 3 and S1). Within the intermediate nTS, ChAT-GFP immunofluorescence extends to include motor nerve root fibers that apparently originate within the DMX (Figs. 3 and S1, i1, magenta). At the i3 – i4 level, ChAT-GFP labels a circular area of neuropil, apparently contained within, but not encompassing all of, the Ce (central) subnucleus of Ganchrow *et al.*, (2014). Finally, heavy

ChAT-GFP immunoreactivity occurs throughout the entire hypoglossal nucleus as evident at intermediate levels of nTS i2 – i5 (Figs. 3 and S1, magenta). The somatic and dendritic ChAT staining clearly demarcates the boundary between the nTS and the more medial and ventral DMX.

### NPY

NPY-immunoreactive fibers and terminals are distributed in the medial part of the nTS roughly coincident with and surrounding the location of the ChAT-positive cells and processes of the DMX (Figs. 4 and S2). At rostral levels, this includes the rostromedial nucleus of Ganchrow et al., (2014). In intermediate nTS levels i1- i3, heavy NPY staining occurs in the medial nTS, primarily in areas of the nTS that border the fourth ventricle, and in the RC subnucleus of Ganchrow et al., (2014). In the intermediate i4 and i5 levels of the nTS, NPY label is sparse, with the densest immunoreactivity lying within DMX of the i5 level. With the exception of dense NPY-immunoreactivity in the AP, few labeled NPY+ fibers occur throughout the remainder of the nTS (Figs. 4 and S2).

### Galanin

Galanin+ fibers have a distribution roughly similar to that of NPY (Figs. 5 and S3), although the peptides do not appear to co-localize within the majority of individual fibers (Fig. 6). Numerous galanin+ fibers distribute within the rostromedial subnucleus and DMX. More caudally, at levels i2- i4, a dense plexus of galaninergic fibers fill the neuropil of the parvocellular subnucleus. Like NPY+ fibers, galanin+ fibers heavily innervate the dorsal aspects of the AP as well.

### CGRP

CGRP is expressed by polymodal nociceptor fibers of the oropharyngeal mucosal afferent nerves including trigeminal and glossopharyngeal nerves (Silverman and Kruger, 1989; Hayakawa *et al.*, 2010; Hayakawa *et al.*, 2014) as well as by a large population of primary vagal viscerosensory neurons (Chery-Croze *et al.*, 1988; Hayakawa *et al.*, 2009; Hayakawa *et al.*, 2014). Numerous CGRP-positive fibers course through the descending trigeminal tract throughout the length of the medulla and many of these terminate locally within the component trigeminal subnuclei (Kruger *et al.*, 1988). A small fascicle of CGRP+ fibers continues medially past the pars oralis of the spinal trigeminal complex to reach the dorsomedial nucleus of the descending trigeminal complex (DMSp5) -- a region sandwiched between the nTS proper and the junction of the pars oralis and pars interpolaris of the trigeminal complex (r2 – i1; Figs. 7 – 8 and S4). Many CGRP+ fibers continue past the DMSp5 to run alongside of and intermingle with the P2X<sub>2</sub>+ fibers along the dorsolateral margin of the nTS (Figs. 7 and S4, magenta). CGRP-immunoreactive puncta and preterminal processes appear both within the DMSp5 and within the nTS itself, filling the neuropil within the RL zone as delimited by the heavy P2X<sub>2</sub>-immunoreactivity in the adjacent RC subdivision. A substantial number of CGRP+ fibers also terminate within the RC, overlapping with the P2X<sub>2</sub> terminal field (r1-r3; Figs. 7 and S4). The overlapped areas are however, not exactly congruent. The CGRP terminal zone is most dense only over the lateral half of the P2X<sub>2</sub> terminal field in the rostral nTS, although sparser CGRP+ fibers do extend more medially. In addition, a unique CGRP+ zone occurs lateral of the rostralateral P2X<sub>2</sub>

fiber area in the rostral nTS. This CGRP+ terminal field extends laterally beyond the nominal boundaries of the nTS and comes to occupy the DMSp5. As described in previous studies (e.g. Marfurt and Rajchert, 1991; Corson *et al.*, 2012); this juxtalimentary CGRP + zone in DMSp5 is within the projection territory of mandibular branch trigeminal primary afferents (Fig. 8).

More caudally within nTS (i2- i5; Figs. 8 and S4), at the level of entrance of vagal nerve roots, numerous CGRP+ fascicles enter the lateral edge of the nTS and form a heavy CGRP + terminal field along the dorsomedial edge of the nucleus, including parts of both the PC (parvicellular) and M (medial) subnuclei at the level of the obex. Scattered CGRP+ fibers and terminals also occur dorsally within the area postrema.

### Sour-Evoked c-Fos/ CGRP Activity in WT and ‘Taste Blind (P2XdbIKO) Mice

Overall, water stimulation evoked few c-Fos positive cells (Fig. 9) within the nTS. Moreover, for P2X WT mice, the total number of water-evoked c-Fos positive cells (i.e., ‘raw’ count) was significantly less than the total number of citric acid-evoked c-Fos positive cells in the nTS ( $347.5 \pm 54.5$  for water;  $717.7 \pm 20.2$  for citric acid; [F (1, 6) = 68.05,  $p < 0.001$ ; c.f. Fig. 9 & 10). In contrast, for P2X-dblKO mice, the total number of water-evoked and citric acid-evoked c-Fos positive cells was similar ( $247 \pm 54.5$  for water vs.  $255.5 \pm 14.7$  citric acid; [F (1, 5) = 0.04,  $p = 0.85$ ).

Citric acid-specific cell counts (raw count – avg. water count) are substantial throughout the entire rostral-caudal nTS of P2X WT mice (i.e. ‘taste normal’), with c-Fos immunoreactivity (Fos-LI) densest in the central region of r3 – i3 and extending laterally at i1 – i3 (Figs. 10 – 13). Moreover, Fos-LI is also present in CGRP+ areas of the lateral nTS, as well as within the neuropil immediately adjacent to the lateral nTS (including DMSp5) and in well-characterized CGRP-rich areas of the caudal part of the spinal trigeminal complex (SP5) and the compact subnucleus of nucleus ambiguus (Nuc. Amb.; Fig.11). However, because c-Fos protein is confined to the nucleus of activated cells, it is difficult to determine whether c-Fos positive neurons receive direct contact from CGRP + fibers. Nevertheless, as shown in Fig. 10, citric acid-evoked Fos-LI occurs in both areas that contain CGRP punctate immunoreactivity (likely terminal endings; yellow arrows), as well as in areas with apparent CGRP+ fibers (blue arrows).

In contrast, in P2X-dbl KO (i.e. ‘taste blind’) mice, citric acid-specific Fos-LI is greatly reduced in most areas of the nTS (Figs. 10 – 13). In particular, the total number of citric acid-specific c-Fos positive-cells is significantly lower in P2X-dbl KO mice than in WT mice ( $370.0 \pm 20.2$  for WT vs.  $-6.7 \pm 14.7$  for P2X-dbl KO; [F (1, 9) = 194.2,  $p < 0.001$ ]). Moreover, this pattern occurs throughout all representative nTS levels (e.g. r1, r2) with Fos-LI significantly less for P2X-dbl KO mice versus WT controls within all nTS levels ([F (8, 72) = 3.6,  $p < 0.001$ ]; all post hoc comparisons  $p < 0.05$ ; Fig. 11).

However, within the CGRP-rich DMSp5, SP5, and Nuc. Amb., citric acid-specific Fos-LI cell numbers are similar to that observed within the brain stem of P2X WT animals ([F (8, 72) = 0.48,  $p = 0.87$ ]; Figs. 10 – 13). Similarly, in the CGRP+ rich areas of the lateral subdivision of nTS (levels r3- i2), although the number of citric-acid specific c-Fos

expressing cells is reduced compared to WT, these numbers are substantially above background. Together, these data suggest that polymodal nociceptors that innervate the oropharynx, as marked by CGRP fiber immunoreactivity, or a related non-gustatory fiber system may be responsible for induction of c-Fos upon oral stimulation by acids even in the absence of taste function.

## Discussion

Multiple primary afferent systems innervating the oropharynx and esophagus project centrally into the dorsolateral quadrant of the medulla, including the nTS and trigeminal brainstem complex. Traditionally, the nTS is considered to be the primary viscerosensory nucleus mediating taste functions while the descending trigeminal complex is considered to be a primary somatosensory nucleus conveying information about touch, pain and temperature. Yet the lingual branch of the trigeminal nerve projects to both of these regions (Corson *et al.*, 2012) and neurons within the nTS respond to multiple physical as well as chemical stimuli applied to the oral cavity (Ogawa *et al.*, 1984; Hayama *et al.*, 1985; Halsell *et al.*, 1996; Wilson and Lemon, 2013; Breza and Travers, 2016). Further complicating the situation is a lack of a clear cytoarchitectonic boundary delineating the nTS from the DMSp5 subnucleus of the medullary trigeminal complex. Thus, we utilized immunohistochemistry and activity mapping with c-Fos in an attempt to define some of these boundaries and subnuclei in the current study.

The nTS is a complex column within the dorsal medulla serving as the terminus of diverse viscerosensory primary afferents from the facial, glossopharyngeal, and vagus nerves. The general visceral components of these afferent systems, largely conveyed by the vagus nerve, terminate in cytologically and molecularly definable regions of the caudal portion of the solitary complex (Calingasan and Ritter, 1992; Berk *et al.*, 1993; Sykes *et al.*, 1994). In contrast, the special viscerosensory component, i.e. taste, targets the dorsal and lateral subdivisions of the rostral nTS, which are relatively more difficult to distinguish and are continuous respectively laterally and ventrally with adjacent trigeminal nuclei and the reticular formation.

While several of the more lateral and rostral portions of the nTS remain poorly differentiated in terms of cytology, staining for P2X<sub>2</sub> and CGRP allows us to distinguish several of the subnuclei in the dorsal nTS. Immunohistochemistry for P2X<sub>2</sub>, which stains primary gustatory and viscerosensory afferents, delineates the boundary between the RC and RL subnuclei of the nTS (Breza and Travers, 2016). In contrast, staining for CGRP, which marks a population of trigeminal polymodal nociceptors, lies within both of these dorsal subnuclei as well as the laterally adjacent DMSp5. The other markers employed in this study, e.g. NPY, galanin and ChAT, were not useful in defining functional domains within the rostral and lateral nTS, although they did delineate medial and caudal subnuclei of the complex.

Whereas these other markers were not useful in delimiting taste-related subnuclei, they may serve as indirect markers of afferent and efferent circuitry with the nTS and adjacent areas. For instance, both the DMX and medial subnucleus of the nTS receive projections from the

hypothalamus (Rogers *et al.*, 1980; van der Kooy *et al.*, 1984; Berthoud and Munzberg, 2011), which contains numerous peptidergic systems involved in regulation of feeding. However, it is unclear whether these hypothalamic peptidergic systems project into the gustatory portions of the nTS. Moreover, we did not observe any NPY or galanin + cell bodies within the brainstem, suggesting that the cell bodies for these immunoreactive fibers lie in other areas, such as in the caudal nTS (where, at least respect to galanin, immunoreactive cell bodies are well documented; Herbert and Saper, 1990). Alternatively, rapid transport of peptides from the soma into the axons and terminal endings may account for the lack of NPY and galanin staining in cell bodies in our study.

### Acid-induced c-Fos activity

Intraoral injection of mildly acidic solutions evokes sensations of sourness and, at slightly higher concentrations, a sense of tingling bordering on irritation. These sensations are commonly attributed respectively to the sense of taste (sour) and general mucosal innervation (tingling, irritation) now referred to as chemesthesis (Green, 2012). The sense of taste depends on neurotransmission from taste buds to afferent fibers via the purinergic receptors P2X<sub>2</sub> and P2X<sub>3</sub> (Finger *et al.*, 2005). In particular, genetic deletion of these receptors (in P2X-dbl KO mice) abolishes all taste-related activity in the chorda tympani, a pure taste nerve, although residual activity remains in the glossopharyngeal and superior laryngeal nerves (Ohkuri *et al.*, 2012), which contain an admixture of general mucosal fibers. Interestingly, P2X-dblKO animals retain the ability to respond to acids, but are deficient in responses to all other tastants (Finger *et al.*, 2005; Hallock *et al.*, 2009). In parallel with the lack of taste responsiveness in these physiological and behavioral studies, tastant-induced c-Fos expression in the nTS is markedly reduced in P2X-dblKO animals (Stratford and Finger, 2011) for canonical tastants such as monosodium glutamate, which is both salty and umami.

Introduction of sour (acidic) solutions to the oral cavity in WT mice similarly evokes robust c-Fos activity in neurons of the DMSp5 and rostral nTS. Surprisingly, P2X-dblKO mice, despite the lack of neural taste responses to sour, display significant c-Fos activation in response to citric acid. The location of these citric-acid activated neurons in the P2X-dblKO mice is, however, not as widespread as in the P2X WT mice. In P2X WT animals, many more c-Fos-labeled cells lie in the rostral (r3 – i2; see Figs 10) subdivisions of the nTS than in P2X-dblKO mice although some activated neurons are present here even in the KO animals. This rostral portion of the nTS corresponds to the portion receiving the densest innervation by the chorda tympani and glossopharyngeal nerves (Corson and Erisir, 2013). The residual citric acid-induced c-Fos in this area likely is attributable to trigeminal and general mucosal innervation by the glossopharyngeal nerve delineated by the distribution of CGRP-immunoreactive fibers within the nTS (Sugimoto *et al.*, 1997). This residual citric acid-induced activation, then, may be attributed to continued responsiveness of acid-sensitive trigeminal nerve fibers, e.g. polymodal nociceptors expressing CGRP along with TrpV1 or TrpA1 channels.

Further complicating interpretation of the acid-induced c-Fos is the likelihood of acidic activation of nerve fibers innervating the esophagus once the solution is swallowed.

Esophageal fibers express TRPV1 as well as acid-sensing ion channels (ASICs; Ma *et al.*, 2011; Vandewauw *et al.*, 2013; Dusenкова *et al.*, 2014). In support of this idea, in wildtype animals, deglutition of citric acid solutions activates neurons in the central nucleus of the nTS, the termination site for esophageal afferents (Wank and Neuhuber, 2001). Moreover, this activity is lost in the nTS of P2X-dblKO mice (Figs. 11 & 12). This might seem odd in that the esophagus has few taste buds, so disruption of taste transmission by elimination of the P2X receptors would not seem likely to disrupt signaling of esophageal acidification by free nerve endings. However, nerve fibers innervating the esophagus do utilize ATP signaling via P2X2/3 receptors to detect ATP released by the esophageal epithelium upon acidification (Kwong *et al.*, 2008; Ma *et al.*, 2011). Hence genetic deletion of the P2X2/3 receptors may block not only taste transmission but also vagal activation due to release of ATP by the esophageal epithelium. Nonetheless, since the P2XdblKO mice do avoid intake of acids in the absence of taste signaling, esophageal fibers are likely not involved in the continued behavioral avoidance in these knockouts since their function too may be disrupted by the genetic deletion of the P2X2/3 receptors.

### Dorsomedial Trigeminal Nuclei (DMSp5)

Evidence for trigeminal responsiveness to the citric acid is offered by the induction of c-Fos in the rostral half of the DMSp5 laterally adjacent to the nTS (Figs. 10 and 11). Cells in this region are activated to a similar degree in the WT and P2X-dblKO lines, indicating a non-gustatory source for this activation. The distinct nature of the DMSp5 was first recognized by Astrom (1953) on the basis of the appearance of preterminal branching patterns of trigeminal fibers and by the intermediate size of cells contained therein – larger than neurons of the nTS, but smaller than those in adjacent trigeminal nuclei and reticular formation. The DMSp5 defined by Astrom lies at the lateral margin of the nTS, extending caudally from roughly the line of transition from pars oralis to pars interpolaris of the brainstem trigeminal complex -- approximately spanning our rostral and intermediate levels of nTS. The DMSp5 receives substantial primary afferent input from only the mandibular branch of the trigeminal nerve, and especially from intraoral as opposed to external facial features even within that branch (Takemura *et al.*, 1987). The region delineated by Astrom is not, however, identical to the DMSp5 as indicated in the Paxinos Atlas (Paxinos and Franklin, 2001; RRID:SCR\_007127), nor is it entirely equivalent to the area of the DMSp5 complex as indicated in the Allen Brain Atlas (Lein *et al.*, 2007; <http://mouse.brain-map.org/>; RRID:SCR\_002978). In particular, both of these atlases show the dorsomedial nucleus as extending farther ventrally than does Astrom. Importantly, CGRP-immunoreactive nerve fibers of the trigeminal nerve extend only into the dorsal region as defined by Astrom (Sugimoto *et al.*, 1997; Matthews *et al.*, 2015) and as shown in the present work. Moreover, it is only this dorsal region that shows citric-acid induced c-Fos. The Allen Brain atlas designates this dorsal, CGRP-rich area as the pars oralis of the dorsomedial complex (SPVomdm). Whether more ventral regions should be designated as part of the dorsomedial nucleus, or simply part of the pars interpolaris is open to question. In any event, as pointed out by many others (e.g. Matthews *et al.*, 2015) the medullary trigeminal nuclear complex is certainly not as simple as the standard textbook tripartite division into pars oralis, pars interpolaris and pars caudalis.

Somewhat complicating this picture is the apparent contribution of CGRP fibers of the glossopharyngeal nerve. Such CGRP-positive fibers enter the lateral aspect of the medulla contributing axons to the descending trigeminal tracts as well as to the NTS (Sugimoto *et al.*, 1997; Corson *et al.*, 2012). CGRP-immunoreactive fibers of the glossopharyngeal nerve richly innervate the lingual and pharyngeal epithelia (Terenghi *et al.*, 1986; Hayakawa *et al.*, 2010; Ohkuri *et al.*, 2012) and include a population of capsaicin-sensitive peptidergic (Terenghi *et al.*, 1986; Hayakawa *et al.*, 2010) polymodal nociceptors, which likely would be responsive to oral acidification. These fibers may then account for the remaining activation of neurons at midlevels (r4-i4) of the nTS in the P2X-dblKO animals.

## Conclusions

Together our results demonstrate that exposures of the oral cavity to acidic solutions evoke substantial taste-related activity within the nTS. In addition, in the absence of a functional taste system, significant activation occurs both within nTS and the DMSp5. We suggest that the residual non-taste activation within these nuclei is attributable to acid-responsive sensory fibers of the trigeminal and glossopharyngeal nerves that innervate the oropharyngeal mucosae.

## Supplementary Material

Refer to Web version on PubMed Central for supplementary material.

## Acknowledgments

The authors thank Debra Cockayne and Roche Palo Alto (Palo Alto, CA) for providing the WT and P2X-dblKO mice, and Afferent Pharmaceuticals (San Mateo, California), for allowing continued utilization of these mice. Also, special thanks to Jason Parnes and Nicole Shultz for immunohistochemistry and other technical support. This work was supported by an NIH grants to JMS (5F32DC012025-03), to Dr. Thomas E. Finger (5R01DC012931-03) and the Rocky Mountain Taste and Smell Center (P30 DC04657).

## References

- Altschuler SM, Bao XM, Bieger D, Hopkins DA, Miselis RR. Viscerotopic representation of the upper alimentary tract in the rat: sensory ganglia and nuclei of the solitary and spinal trigeminal tracts. *J Comp Neurol.* 1989; 283(2):248–268. [PubMed: 2738198]
- Archer S, Li TT, Evans AT, Britland ST, Morgan H. Cell reactions to dielectrophoretic manipulation. *Biochem Biophys Res Commun.* 1999; 257(3):687–698. [PubMed: 10208845]
- Astrom KE. On the central course of afferent fibers in the trigeminal, facial, glossopharyngeal, and vagal nerves and their nuclei in the mouse. *Acta physiol. scand., Suppl.* 1953; 29:209–320.
- Bae YC, Oh JM, Hwang SJ, Shigenaga Y, Valtchanoff JG. Expression of vanilloid receptor TRPV1 in the rat trigeminal sensory nuclei. *J Comp Neurol.* 2004; 478(1):62–71. [PubMed: 15334649]
- Bartel DL. Glial responses after chorda tympani nerve injury. *J Comp Neurol.* 2012; 520(12):2712–2729. [PubMed: 22315167]
- Berk ML, Smith SE, Karten HJ. Nucleus of the solitary tract and dorsal motor nucleus of the vagus nerve of the pigeon: localization of peptide and 5-hydroxytryptamine immunoreactive fibers. *J Comp Neurol.* 1993; 338(4):521–548. [PubMed: 8132859]
- Berthoud HR, Munzberg H. The lateral hypothalamus as integrator of metabolic and environmental needs: from electrical self-stimulation to opto-genetics. *Physiol Behav.* 2011; 104(1):29–39. [PubMed: 21549732]
- Bradley, RM. Bradley, RM. *The Role of the Nucleus of the Solitary Tract in Gustatory Processing.* Boca Raton (FL): 2007. rNST Circuits.

- Breza JM, Travers SP. P2X2 Receptor Terminal Field Demarcates a "Transition Zone" for Gustatory and Mechanosensory Processing in the Mouse Nucleus Tractus Solitarius. *Chem Senses*. 2016
- Calingasan NY, Ritter S. Presence of galanin in rat vagal sensory neurons: evidence from immunohistochemistry and in situ hybridization. *J Auton Nerv Syst*. 1992; 40(3):229–238. [PubMed: 1281181]
- Chen Z, Travers SP, Travers JB. Activation of NPY receptors suppresses excitatory synaptic transmission in a taste-feeding network in the lower brain stem. *Am J Physiol Regul Integr Comp Physiol*. 2012; 302(12):R1401–R1410. [PubMed: 22513746]
- Chery-Croze S, Bosshard A, Martin H, Cuber JC, Charnay Y, Chayvialle JA. Peptide immunocytochemistry in afferent neurons from lower gut in rats. *Peptides*. 1988; 9(4):873–881. [PubMed: 3067223]
- Corson J, Aldridge A, Wilmoth K, Erisir A. A survey of oral cavity afferents to the rat nucleus tractus solitarius. *J Comp Neurol*. 2012; 520(3):495–527. [PubMed: 21800298]
- Corson JA, Erisir A. Monosynaptic convergence of chorda tympani and glossopharyngeal afferents onto ascending relay neurons in the nucleus of the solitary tract: a high-resolution confocal and correlative electron microscopy approach. *J Comp Neurol*. 2013; 521(13):2907–2926. [PubMed: 23640852]
- Davis BJ. GABA-like immunoreactivity in the gustatory zone of the nucleus of the solitary tract in the hamster: light and electron microscopic studies. *Brain Res Bull*. 1993; 30(1–2):69–77. [PubMed: 8420636]
- Davis BJ, Smith DV. Substance P modulates taste responses in the nucleus of the solitary tract of the hamster. *Neuroreport*. 1997; 8(7):1723–1727. [PubMed: 9189921]
- Dickman JD, Smith DV. Response properties of fibers in the hamster superior laryngeal nerve. *Brain Res*. 1988; 450(1–2):25–38. [PubMed: 3042090]
- Dusenikova S, Ru F, Surdenikova L, Nassenstein C, Hatok J, Dusenka R, Banovcin P Jr, Kliment J, Tatar M, Kollarik M. The expression profile of acid-sensing ion channel (ASIC) subunits ASIC1a, ASIC1b, ASIC2a, ASIC2b, and ASIC3 in the esophageal vagal afferent nerve subtypes. *Am J Physiol Gastrointest Liver Physiol*. 2014; 307(9):G922–G930. [PubMed: 25190475]
- Eddy MC, Eschle BK, Barrows J, Hallock RM, Finger TE, Delay ER. Double P2X2/P2X3 purinergic receptor knockout mice do not taste NaCl or the artificial sweetener SC45647. *Chem Senses*. 2009; 34(9):789–797. [PubMed: 19833661]
- Eylam S, Moore M, Haskell-Luevano C, Spector AC. Melanocortin-4 receptor-null mice display normal affective licking responses to prototypical taste stimuli in a brief-access test. *Peptides*. 2005; 26(10):1712–1719. [PubMed: 15993983]
- Felizardo R, Boucher Y, Braud A, Carstens E, Dauvergne C, Zerari-Mailly F. Trigeminal projections on gustatory neurons of the nucleus of the solitary tract: a double-label strategy using electrical stimulation of the chorda tympani and tracer injection in the lingual nerve. *Brain Res*. 2009; 1288:60–68. [PubMed: 19595675]
- Finger TE, Danilova V, Barrows J, Bartel DL, Vigers AJ, Stone L, Hellekant G, Kinnamon SC. ATP signaling is crucial for communication from taste buds to gustatory nerves. *Science*. 2005; 310(5753):1495–1499. [PubMed: 16322458]
- Finley JC, Erickson JT, Katz DM. Galanin expression in carotid body afferent neurons. *Neuroscience*. 1995; 68(3):937–942. [PubMed: 8577385]
- Ganchrow D, Ganchrow JR, Cicchini V, Bartel DL, Kaufman D, Girard D, Whitehead MC. Nucleus of the solitary tract in the C57BL/6J mouse: Subnuclear parcellation, chorda tympani nerve projections, and brainstem connections. *J Comp Neurol*. 2014; 522(7):1565–1596. [PubMed: 24151133]
- Green BG. Chemesthesis and the chemical senses as components of a "chemofensor complex". *Chem Senses*. 2012; 37(3):201–206. [PubMed: 22210122]
- Grybko MJ, Hahm ET, Perrine W, Parnes JA, Chick WS, Sharma G, Finger TE, Vijayaraghavan S. A transgenic mouse model reveals fast nicotinic transmission in hippocampal pyramidal neurons. *Eur J Neurosci*. 2011; 33(10):1786–1798. [PubMed: 21501254]

- Guthrie KM, Anderson AJ, Leon M, Gall C. Odor-induced increases in c-fos mRNA expression reveal an anatomical "unit" for odor processing in olfactory bulb. *Proc Natl Acad Sci U S A*. 1993; 90(8): 3329–3333. [PubMed: 8475076]
- Hallock RM, Tatangelo M, Barrows J, Finger TE. Residual chemosensory capabilities in double P2X2/P2X3 purinergic receptor null mice: intraoral or postingestive detection? *Chem Senses*. 2009; 34(9):799–808. [PubMed: 19833662]
- Halsell CB, Travers SP, Travers JB. Ascending and descending projections from the rostral nucleus of the solitary tract originate from separate neuronal populations. *Neuroscience*. 1996; 72(1):185–197. [PubMed: 8730716]
- Hanamori T, Smith DV. Central projections of the hamster superior laryngeal nerve. *Brain Res Bull*. 1986; 16(2):271–279. [PubMed: 3697793]
- Hayakawa T, Kuwahara-Otani S, Maeda S, Tanaka K, Seki M. Calcitonin gene-related peptide immunoreactive sensory neurons in the vagal and glossopharyngeal ganglia innervating the larynx of the rat. *J Chem Neuroanat*. 2014; 55:18–23. [PubMed: 24269509]
- Hayakawa T, Kuwahara S, Maeda S, Tanaka K, Seki M. Distribution of vagal CGRP-immunoreactive fibers in the lower esophagus and the cardia of the stomach of the rat. *J Chem Neuroanat*. 2009; 38(2):124–129. [PubMed: 19691152]
- Hayakawa T, Kuwahara S, Maeda S, Tanaka K, Seki M. Calcitonin gene-related peptide immunoreactive neurons innervating the soft palate, the root of tongue, and the pharynx in the superior glossopharyngeal ganglion of the rat. *J Chem Neuroanat*. 2010; 39(4):221–227. [PubMed: 20034556]
- Hayama T, Ito S, Ogawa H. Responses of solitary tract nucleus neurons to taste and mechanical stimulations of the oral cavity in decerebrate rats. *Exp Brain Res*. 1985; 60(2):235–242. [PubMed: 4054268]
- Herbert H, Saper CB. Cholecystokinin-, galanin-, and corticotropin-releasing factor-like immunoreactive projections from the nucleus of the solitary tract to the parabrachial nucleus in the rat. *J Comp Neurol*. 1990; 293(4):581–598. [PubMed: 1691749]
- Ingham ES, Gunhan E, Fuller PM, Fuller CA. Immunotoxin-induced ablation of melanopsin retinal ganglion cells in a non-murine mammalian model. *J Comp Neurol*. 2009; 516(2):125–140. [PubMed: 19575450]
- Katz DM, Karten HJ. Visceral representation within the nucleus of the tractus solitarius in the pigeon, *Columba livia*. *J Comp Neurol*. 1983; 218(1):42–73. [PubMed: 6886066]
- Kelsch W, Sim S, Lois C. Increasing heterogeneity in the organization of synaptic inputs of mature olfactory bulb neurons gene-rated in newborn rats. *J Comp Neurol*. 2012; 520(6):1327–1338. [PubMed: 22102059]
- King MS. Distribution of immunoreactive GABA and glutamate receptors in the gustatory portion of the nucleus of the solitary tract in rat. *Brain Res Bull*. 2003; 60(3):241–254. [PubMed: 12754086]
- Klein S, Jurkevich A, Grossmann R. Sexually dimorphic immunoreactivity of galanin and colocalization with arginine vasotocin in the chicken brain (*Gallus gallus domesticus*). *J Comp Neurol*. 2006; 499(5):828–839. [PubMed: 17048233]
- Kosaras B, Jakubowski M, Kainz V, Burstein R. Sensory innervation of the calvarial bones of the mouse. *J Comp Neurol*. 2009; 515(3):331–348. [PubMed: 19425099]
- Kruger L, Sternini C, Brecha NC, Mantyh PW. Distribution of calcitonin gene-related peptide immunoreactivity in relation to the rat central somatosensory projection. *J Comp Neurol*. 1988; 273(2):149–162. [PubMed: 3047185]
- Kwong K, Kollarik M, Nassenstein C, Ru F, Udem BJ. P2X2 receptors differentiate placodal vs. neural crest C-fiber phenotypes innervating guinea pig lungs and esophagus. *Am J Physiol Lung Cell Mol Physiol*. 2008; 295(5):L858–L865. [PubMed: 18689601]
- Lein ES, Hawrylycz MJ, Ao N, Ayres M, Bensinger A, Bernard A, Boe AF, Boguski MS, Brockway KS, Byrnes EJ, Chen L, Chen L, Chen TM, Chin MC, Chong J, Crook BE, Czaplinska A, Dang CN, Datta S, Dee NR, Desaki AL, Desta T, Diep E, Dolbeare TA, Donelan MJ, Dong HW, Dougherty JG, Duncan BJ, Ebbert AJ, Eichele G, Estin LK, Faber C, Facer BA, Fields R, Fischer SR, Fliss TP, Frensley C, Gates SN, Glattfelder KJ, Halverson KR, Hart MR, Hohmann JG, Howell MP, Jeung DP, Johnson RA, Karr PT, Kawal R, Kidney JM, Knapik RH, Kuan CL, Lake

JH, Laramée AR, Larsen KD, Lau C, Lemon TA, Liang AJ, Liu Y, Luong LT, Michaels J, Morgan JJ, Morgan RJ, Mortrud MT, Mosqueda NF, Ng LL, Ng R, Orta GJ, Overly CC, Pak TH, Parry SE, Pathak SD, Pearson OC, Puchalski RB, Riley ZL, Rockett HR, Rowland SA, Royall JJ, Ruiz MJ, Sarno NR, Schaffnit K, Shapovalova NV, Sivasay T, Slaughterbeck CR, Smith SC, Smith KA, Smith BI, Sodr AJ, Stewart NN, Stumpf KR, Sunkin SM, Sutram M, Tam A, Teemer CD, Thaller C, Thompson CL, Varnam LR, Visel A, Whitlock RM, Wohnoutka PE, Wolkey CK, Wong VY, Wood M, Yaylaoglu MB, Young RC, Youngstrom BL, Yuan XF, Zhang B, Zwingman TA, Jones AR. Genome-wide atlas of gene expression in the adult mouse brain. *Nature*. 2007; 445(7124): 168–176. [PubMed: 17151600]

- Ma J, Altomare A, Rieder F, Behar J, Biancani P, Harnett KM. ATP: a mediator for HCl-induced TRPV1 activation in esophageal mucosa. *Am J Physiol Gastrointest Liver Physiol*. 2011; 301(6):G1075–G1082. [PubMed: 21960521]
- Marfurt CF, Rajchert DM. Trigeminal primary afferent projections to "non-trigeminal" areas of the rat central nervous system. *J Comp Neurol*. 1991; 303(3):489–511. [PubMed: 1706735]
- Matthews DW, Deschenes M, Furuta T, Moore JD, Wang F, Karten HJ, Kleinfeld D. Feedback in the brainstem: an excitatory disynaptic pathway for control of whisking. *J Comp Neurol*. 2015; 523(6):921–942. [PubMed: 25503925]
- Ogawa H, Imoto T, Hayama T. Responsiveness of solitario-parabrachial relay neurons to taste and mechanical stimulation applied to the oral cavity in rats. *Exp Brain Res*. 1984; 54(2):349–358. [PubMed: 6723854]
- Ohkuri T, Horio N, Stratford JM, Finger TE, Ninomiya Y. Residual chemoresponsiveness to acids in the superior laryngeal nerve in "taste-blind" (P2X2/P2X3 double-KO) mice. *Chem Senses*. 2012; 37(6):523–532. [PubMed: 22362867]
- Paxinos, G.; Franklin, KBJ. *The mouse brain in stereotaxic coordinates*. San Diego: Academic Press; 2001.
- Rogers RC, Kita H, Butcher LL, Novin D. Afferent projections to the dorsal motor nucleus of the vagus. *Brain Res Bull*. 1980; 5(4):365–373. [PubMed: 7407633]
- Rogers RC, McCann MJ. Intramedullary connections of the gastric region in the solitary nucleus: a biocytin histochemical tracing study in the rat. *J Auton Nerv Syst*. 1993; 42(2):119–130. [PubMed: 8450172]
- Silverman JD, Kruger L. Calcitonin-gene-related-peptide-immunoreactive innervation of the rat head with emphasis on specialized sensory structures. *J Comp Neurol*. 1989; 280(2):303–330. [PubMed: 2784449]
- Stratford JM, Finger TE. Central representation of postingestive chemosensory cues in mice that lack the ability to taste. *J Neurosci*. 2011; 31(25):9101–9110. [PubMed: 21697361]
- Stratford JM, Thompson JA. MSG-Evoked c-Fos Activity in the Nucleus of the Solitary Tract Is Dependent upon Fluid Delivery and Stimulation Parameters. *Chem Senses*. 2016; 41(3):211–220. [PubMed: 26762887]
- Sugimoto T, Fujiyoshi Y, Xiao C, He YF, Ichikawa H. Central projection of calcitonin gene-related peptide (CGRP)- and substance P (SP)-immunoreactive trigeminal primary neurons in the rat. *J Comp Neurol*. 1997; 378(3):425–442. [PubMed: 9034901]
- Sykes RM, Spyer KM, Izzo PN. Central distribution of substance P, calcitonin gene-related peptide and 5-hydroxytryptamine in vagal sensory afferents in the rat dorsal medulla. *Neuroscience*. 1994; 59(1):195–210. [PubMed: 7514769]
- Takemura M, Sugimoto T, Sakai A. Topographic organization of central terminal region of different sensory branches of the rat mandibular nerve. *Exp Neurol*. 1987; 96(3):540–557. [PubMed: 3582543]
- Terenghi G, Polak JM, Rodrigo J, Mulderry PK, Bloom SR. Calcitonin gene-related peptide-immunoreactive nerves in the tongue, epiglottis and pharynx of the rat: occurrence, distribution and origin. *Brain Res*. 1986; 365(1):1–14. [PubMed: 3512035]
- Usoskin D, Furlan A, Islam S, Abdo H, Lonnerberg P, Lou D, Hjerling-Leffler J, Haeggstrom J, Kharchenko O, Kharchenko PV, Linnarsson S, Ernfors P. Unbiased classification of sensory neuron types by large-scale single-cell RNA sequencing. *Nat Neurosci*. 2015; 18(1):145–153. [PubMed: 25420068]

- Uteshev VV, Smith DV. Cholinergic modulation of neurons in the gustatory region of the nucleus of the solitary tract. *Brain Res.* 2006; 1084(1):38–53. [PubMed: 16546141]
- van der Kooy D, Koda LY, McGinty JF, Gerfen CR, Bloom FE. The organization of projections from the cortex, amygdala, and hypothalamus to the nucleus of the solitary tract in rat. *J Comp Neurol.* 1984; 224(1):1–24. [PubMed: 6715573]
- Vandewauw I, Owsianik G, Voets T. Systematic and quantitative mRNA expression analysis of TRP channel genes at the single trigeminal and dorsal root ganglion level in mouse. *BMC Neurosci.* 2013; 14:21. [PubMed: 23410158]
- Wang M, Bradley RM. Properties of GABAergic neurons in the rostral solitary tract nucleus in mice. *J Neurophysiol.* 2010; 103(6):3205–3218. [PubMed: 20375246]
- Wank M, Neuhuber WL. Local differences in vagal afferent innervation of the rat esophagus are reflected by neurochemical differences at the level of the sensory ganglia and by different brainstem projections. *J Comp Neurol.* 2001; 435(1):41–59. [PubMed: 11370010]
- Whitehead MC. Neuronal architecture of the nucleus of the solitary tract in the hamster. *J Comp Neurol.* 1988; 276(4):547–572. [PubMed: 2461969]
- Whitehead MC. Subdivisions and neuron types of the nucleus of the solitary tract that project to the parabrachial nucleus in the hamster. *J Comp Neurol.* 1990; 301(4):554–574. [PubMed: 2177063]
- Whitehead, MC.; Finger, TE. Basbaum, AI. *The senses : a comprehensive reference.* Vol. 4. Amsterdam ; Boston: Elsevier; 2008. Gustatory Pathways in Fish and Mammals; p. 237-260.
- Wilson DM, Lemon CH. Modulation of central gustatory coding by temperature. *J Neurophysiol.* 2013; 110(5):1117–1129. [PubMed: 23761701]

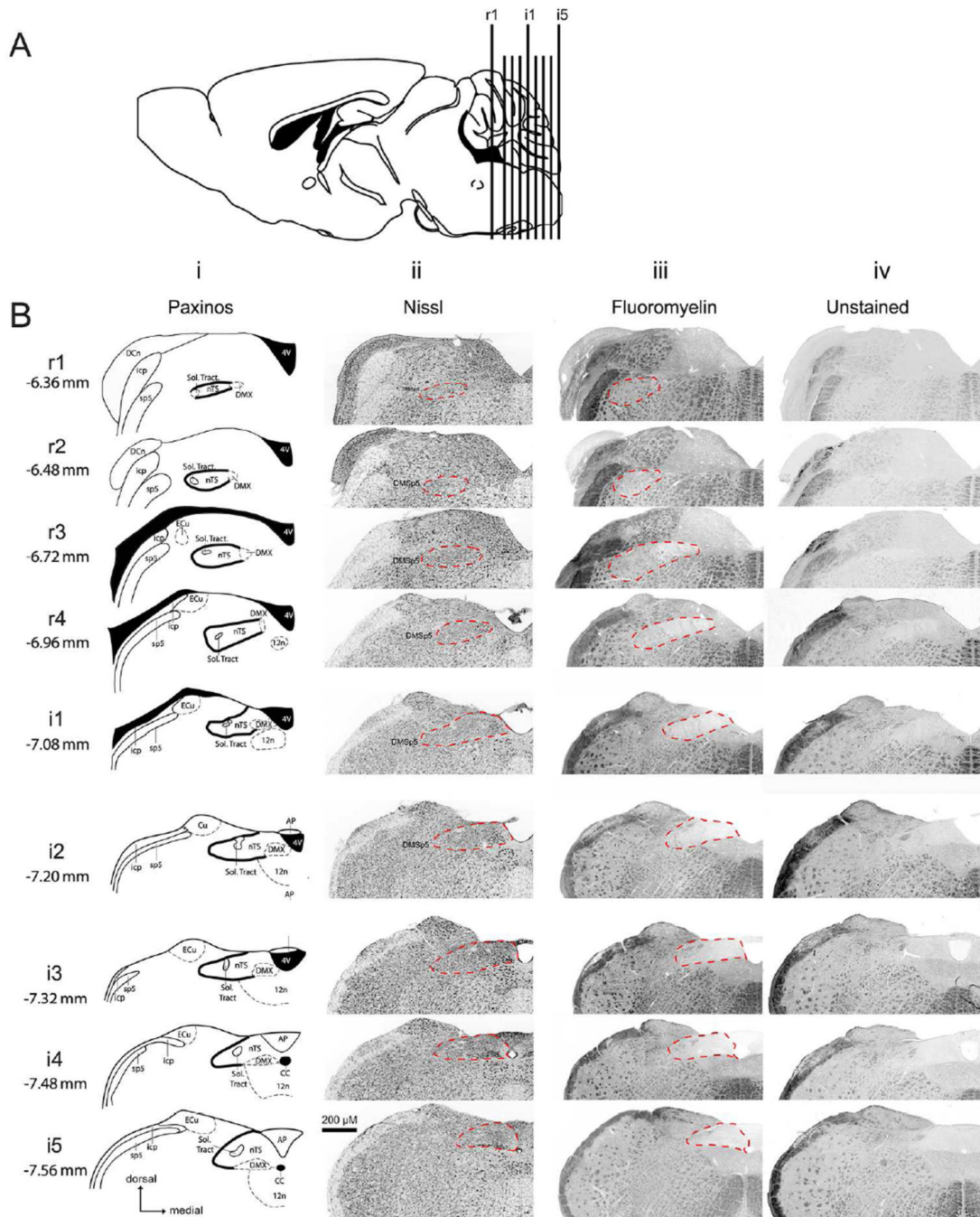


**Figure 1. Rostral-caudal boundaries of nTS based on various staining methodologies**

**A:** Nine standard transverse section planes as projected onto a parasagittal section of a mouse brain. **B:** Nine rostrocaudal nTS levels designated as rostral (r1 – r4) and intermediate (i1- i5). Coordinates from Bregma are listed for each nTS level. For each level the boundary of nTS is indicated to permit comparison between: Column **i**, the Paxinos Atlas (solid black line); Column **ii**, fluorescent Nissl staining (dashed red line); Column **iii**, FluoroMyelin staining (dotted red line); and Column **iv**, Unstained sections (dotted red line). The location of the dorsomedial trigeminal nucleus (DMSp5) is also indicated. Atlas images modified

from 2nd edition of *The Mouse Brain in Stereotaxic Coordinates* (Paxinos and Franklin, 2001).

Author Manuscript

Author Manuscript

Author Manuscript

Author Manuscript

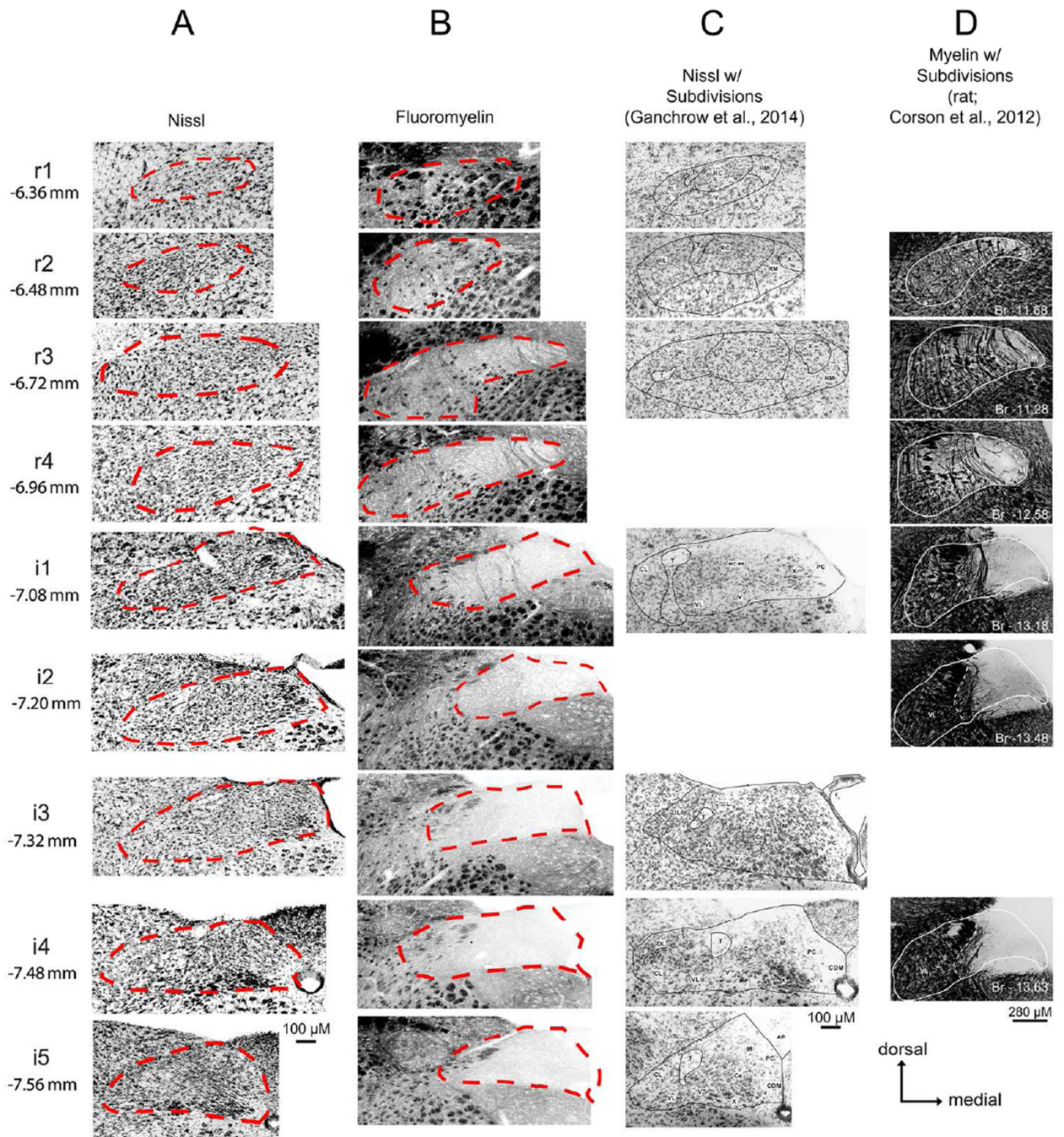


**Figure 2. nTS Boundaries vary significantly not only between staining methodology, but also between published studies**

Photomicrographs of mice (A–C) and rat (D) brainstem sections stained using various methodologies (A. fluorescent nissl; B. FluoroMyelin; C. chromogenic Nissl; D. myelin). For A and B: nTS boundaries are denoted as red dotted lines. For C: nTS boundaries, including nTS subregions are denoted as solid black lines. For D: nTS boundaries are shown as a solid white line. In C and D, images that did not correspond to one of the nine standard nTS levels described in the current study were omitted. Images in C, are reproduced from

Ganchrow *et al.*, 2014 (with permission from Wiley Periodicals, Inc. Copyright © 2013) from the following figures: r1 = Fig. 1A; r2 = Fig. 1C; r3 = Fig. 1E; i1 = Fig. 1G; i3 = Fig. 1I; i4 = Fig. 1K; i5 = Fig. 1M). In **D**, images are reproduced from Corson *et al.*, 2012 (with permission from Wiley-Liss, Inc. Copyright © 2011) from the following figures: r2 = Fig. 3A; r3 = Fig. 3E; r4 = Fig. 3G; i1 = Fig. 4C; i2 = Fig. 4E; i4 = Fig. 4G. Images in D are flipped horizontally from the originals to lie in the same orientation as the other photomicrographs in this figure.

Author Manuscript

Author Manuscript

Author Manuscript

Author Manuscript

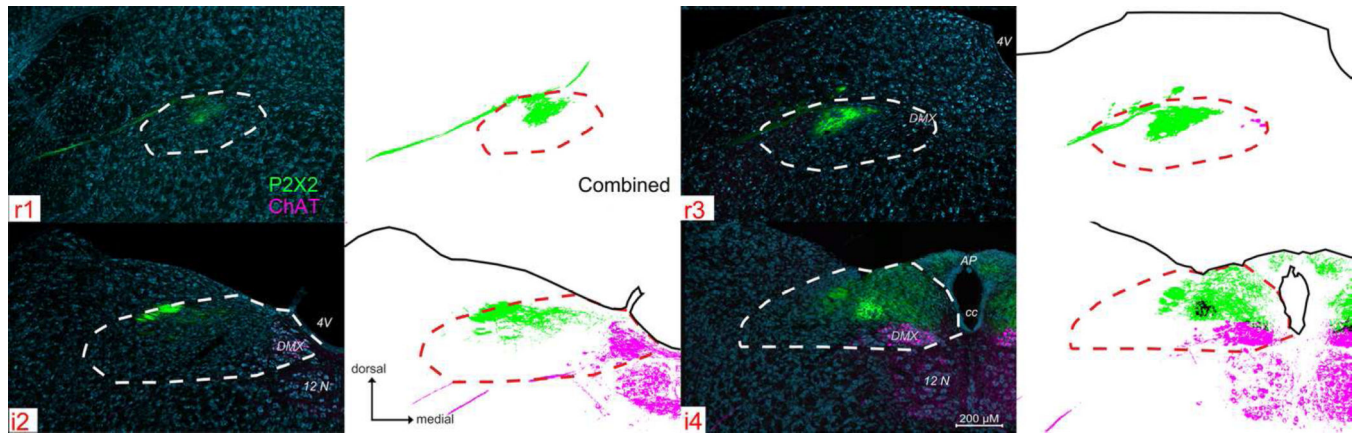


**Figure 3. P2X<sub>2</sub> (green) immunoreactivity and ChAT-GFP (magenta) within four representative nTS levels (r1, r1, i2, i4)**

See supplemental Fig. 1 (S1) for P2X<sub>2</sub>/ChAT immunoreactivity across all nine nTS levels.

For each nTS level, a pair of images is shown, Left: photographs of P2X<sub>2</sub> (green), ChAT (magenta), and a Nissl background stain (cyan), with nTS boundaries indicated as white dotted lines; Right: computationally extracted chartings of the image for each pixel greater than 2 S.D. of background staining. **r1**: In rostral sections, P2X<sub>2</sub> immunoreactive fibers (green) label the facial nerve root as it passes medially through the dorsal medulla, terminating within the dorsocentral subnucleus of the nTS (**r1 & r3**). At more caudal levels (**i2 – i4**), P2X<sub>2</sub> immunoreactive fibers expand medially and ventrally to terminate within the medial two-thirds of the nTS. CHAT- GFP primarily labels brainstem motor nuclei and nerve roots throughout the medulla (including DMX, 12n).

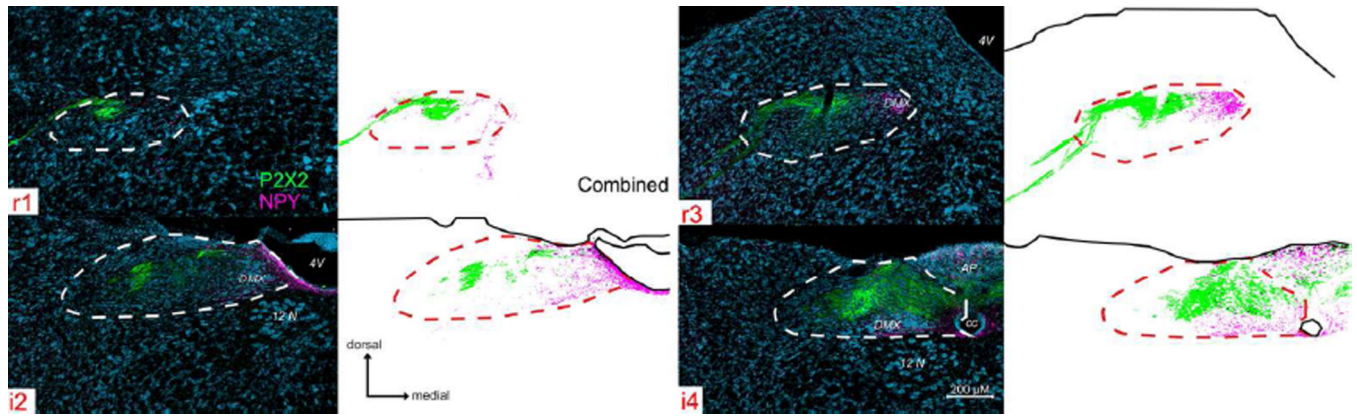


**Figure 4. P2X<sub>2</sub> (green) and NPY (magenta) immunoreactivity across four representative nTS levels**

See supplemental Fig. 2 (S2) for P2X<sub>2</sub>/NPY immunoreactivity across all nine nTS levels. In rostral nTS, NPY-immunoreactive fibers are distributed in the medial part of the nTS and within the DMX in areas that also contain ChAT-positive cells and processes. In intermediate nTS, NPY staining is densest lining the 4<sup>th</sup> ventricle (4V), but also occurs within the area postrema (AP). The nTS boundaries and organization of the figure is as described for Fig. 3.

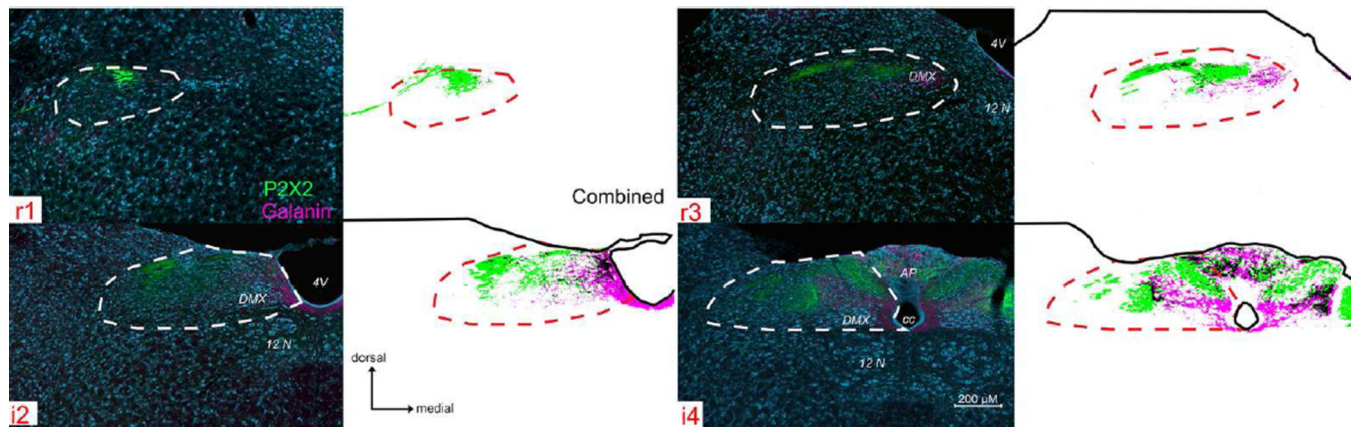


**Figure 5. P2X<sub>2</sub> (green) and galanin (magenta) immunoreactivity across four representative nTS levels**

See supplemental Fig 3. (S3) for P2X<sub>2</sub>/galanin immunoreactivity across all nine nTS levels. Galanin+ fibers are distributed in a roughly similar pattern to that of NPY, although the peptides do not appear to co-localize within the majority of individual fibers (See Fig. 7). The nTS boundaries and organization of the figure is as described for Fig. 3.

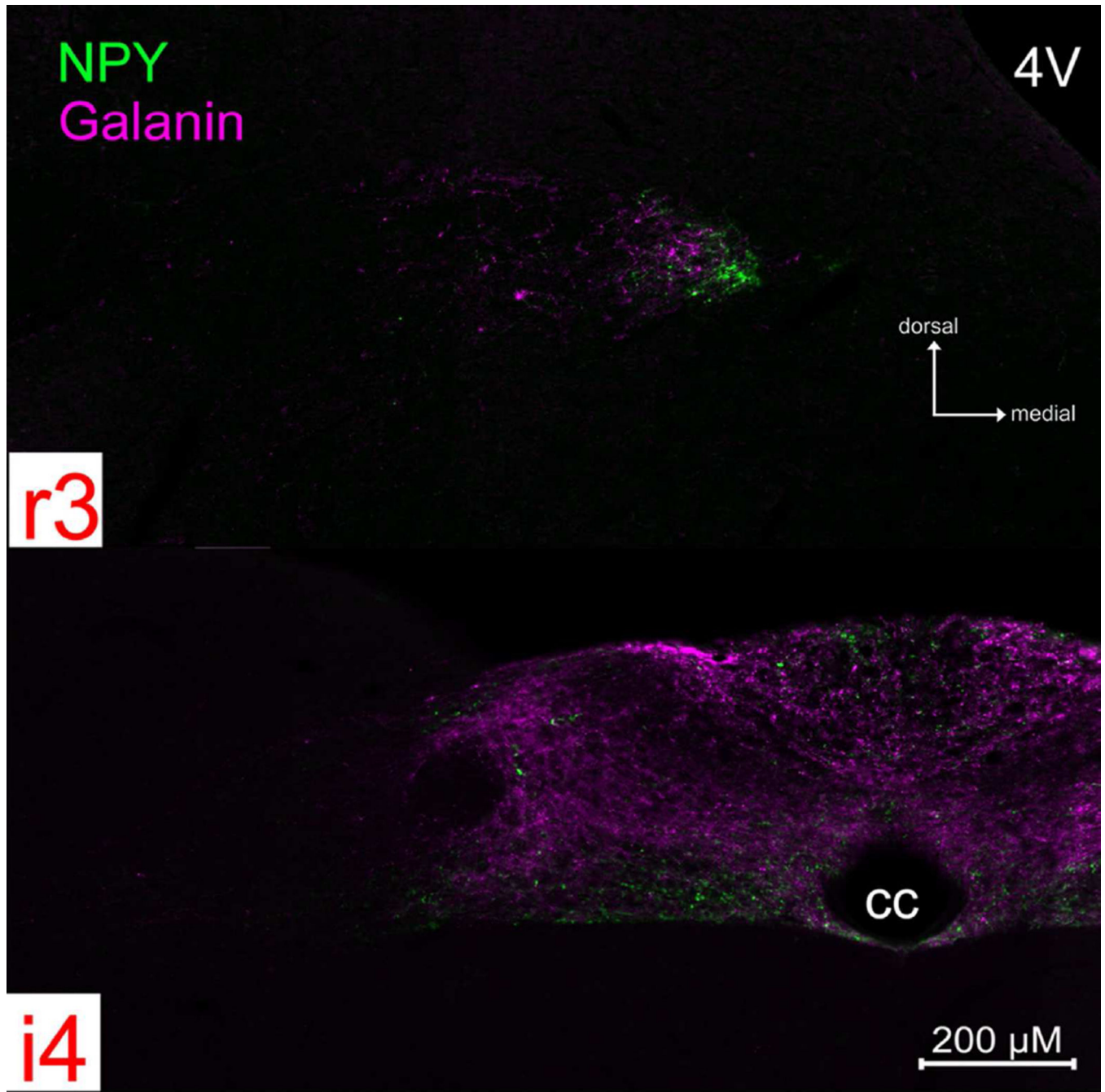


**Figure 6. NPY (green) and galanin (magenta) immunoreactivity do not co-localize in fibers, although their distribution is largely coextensive**  
Photomicrographs of NPY and galanin staining from a rostral (r3) and intermediate (i4) nTS level.

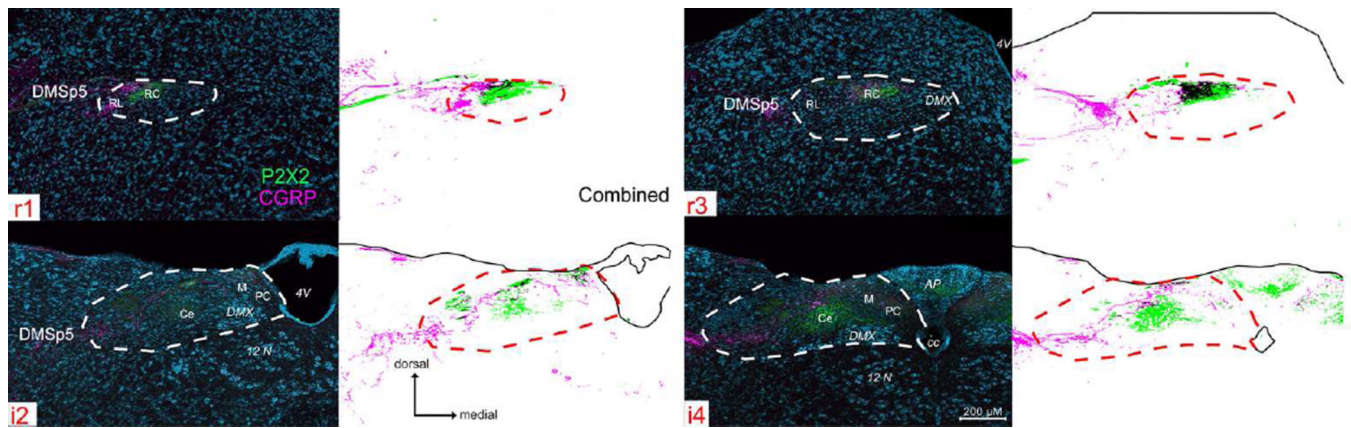


**Figure 7. P2X<sub>2</sub> (green) and CGRP (magenta) immunoreactivity across four representative nTS levels (r1, r3, i2, i4)**

See supplemental Fig. 4 (S4) for P2X<sub>2</sub>/CGRP immunoreactivity across all nine nTS levels.

For each nTS level, a pair of images is shown, Left: photographs of P2X<sub>2</sub> (green), CGRP (magenta), and a Nissl background stain (cyan), with nTS boundaries indicated as white dotted lines; Right: computationally extracted charting of the image for each pixel greater than 2 S.D. of background staining. Patterns of P2X<sub>2</sub> immunoreactivity are similar to that described in Fig. 3 above. CGRP-immunoreactive fibers appear both within and immediately lateral to the RL subdivision of the nTS. However, a substantial number of CGRP+ fibers also terminate within the RC subdivision of nTS, overlapping the P2X<sub>2</sub> terminal field.

Moreover, a unique CGRP+ zone occurs laterally beyond the nominal boundaries of the nTS and occupies the DMSp5.

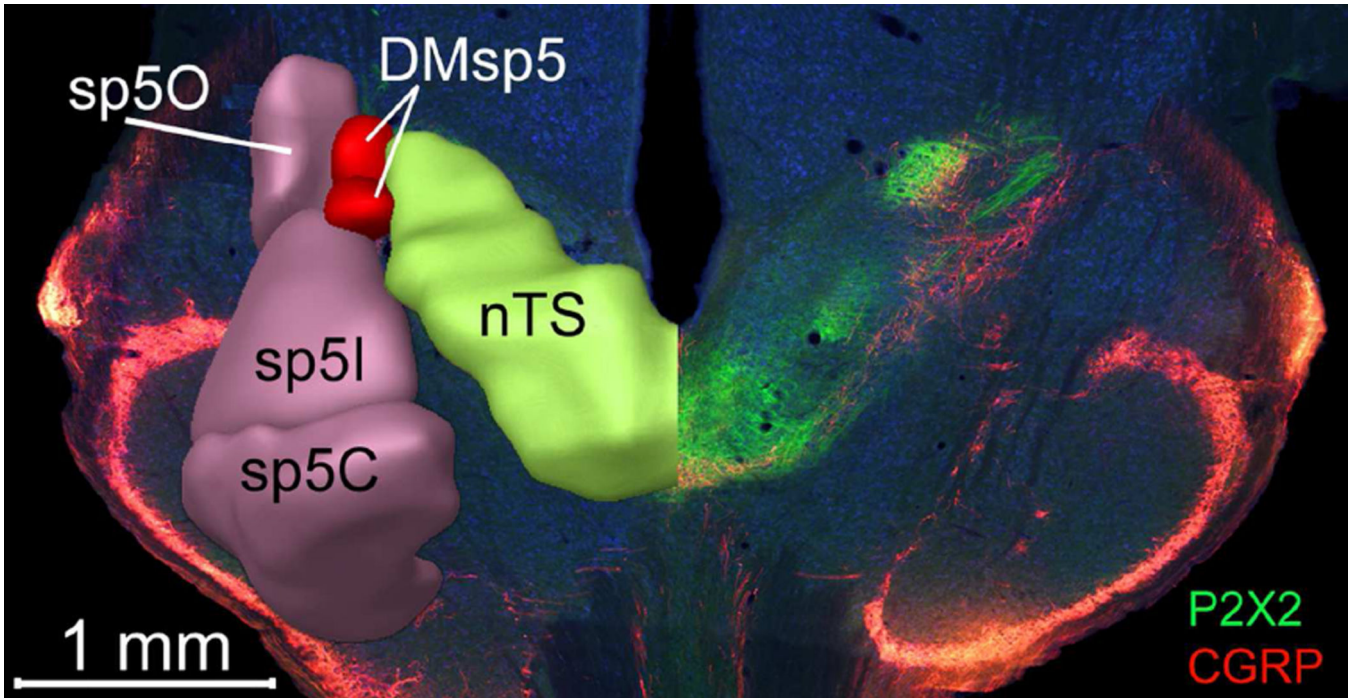


**Figure 8. The dorsomedial trigeminal nucleus (DMSp5) lies between the nucleus of the solitary tract (nTS) proper and the junction of the pars oralis (Sp5O) and pars interpolaris (SP5I) of the trigeminal complex**

Right: As shown in this photomicrograph of a horizontal section through the brainstem P2X<sub>2</sub>-immunoreactive fibers (green), mostly originating from the facial and glossopharyngeal nerves, course caudomedially to terminate throughout the nTS. Fibers immunoreactive for CGRP (red) terminate within portions of the rostral and intermediate nTS as well as in components of the brainstem trigeminal complex including DMSp5. Left: Digital reconstruction of the trigeminal complex and nTS modified from the Allen Brain Institute 'Brain Explorer2' tool (Lein *et al.*, 2007; <http://mouse.brain-map.org/>).

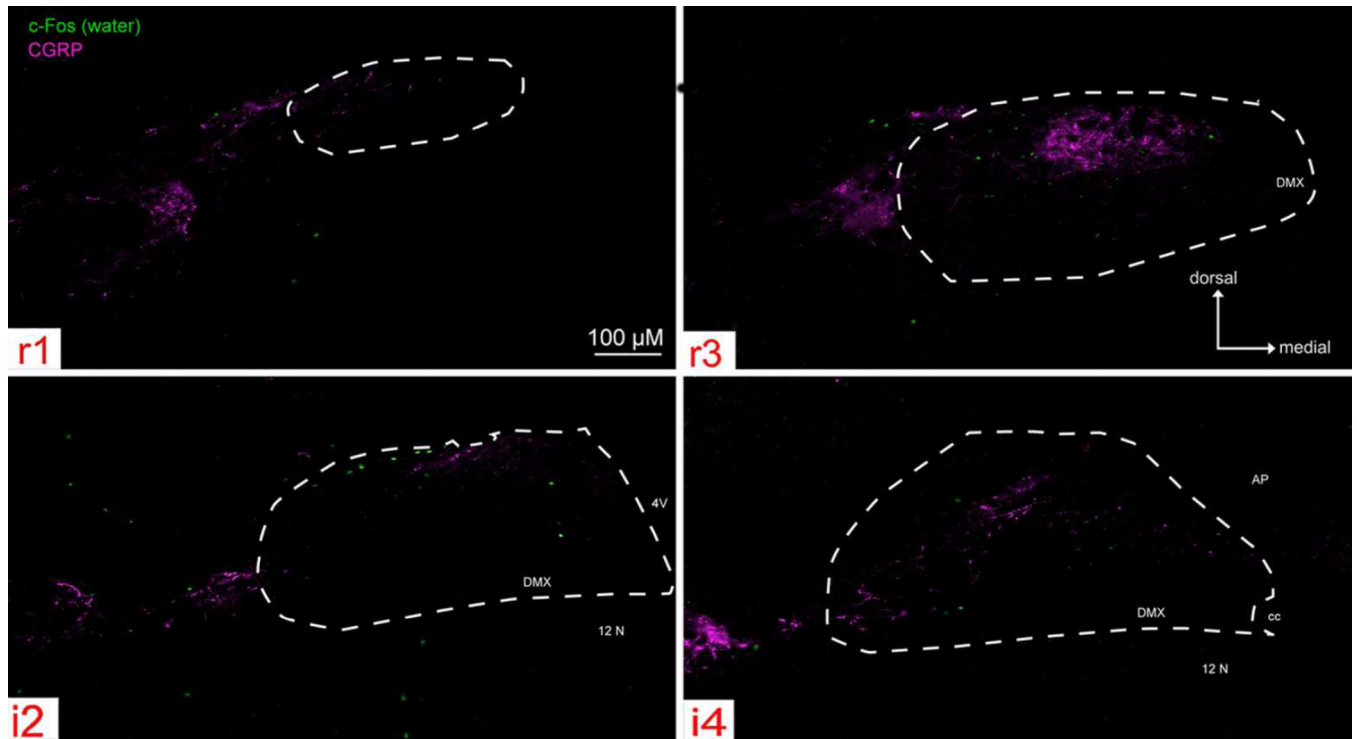


**Figure 9. Water- evoked c-Fos-like Immunoreactivity (Fos-LI) within the brainstem of ‘Control’ (P2X WT) mice across four representative nTS levels (r1, r3, i2, i4)**  
 Photomicrographs of water-evoked c-Fos (green) and CGRP (magenta) staining, with nTS boundaries indicated as white dotted lines. Water stimulation evoked few c-Fos positive cells both within and outside the nTS, and Fos-LI was widely distributed throughout the brainstem.

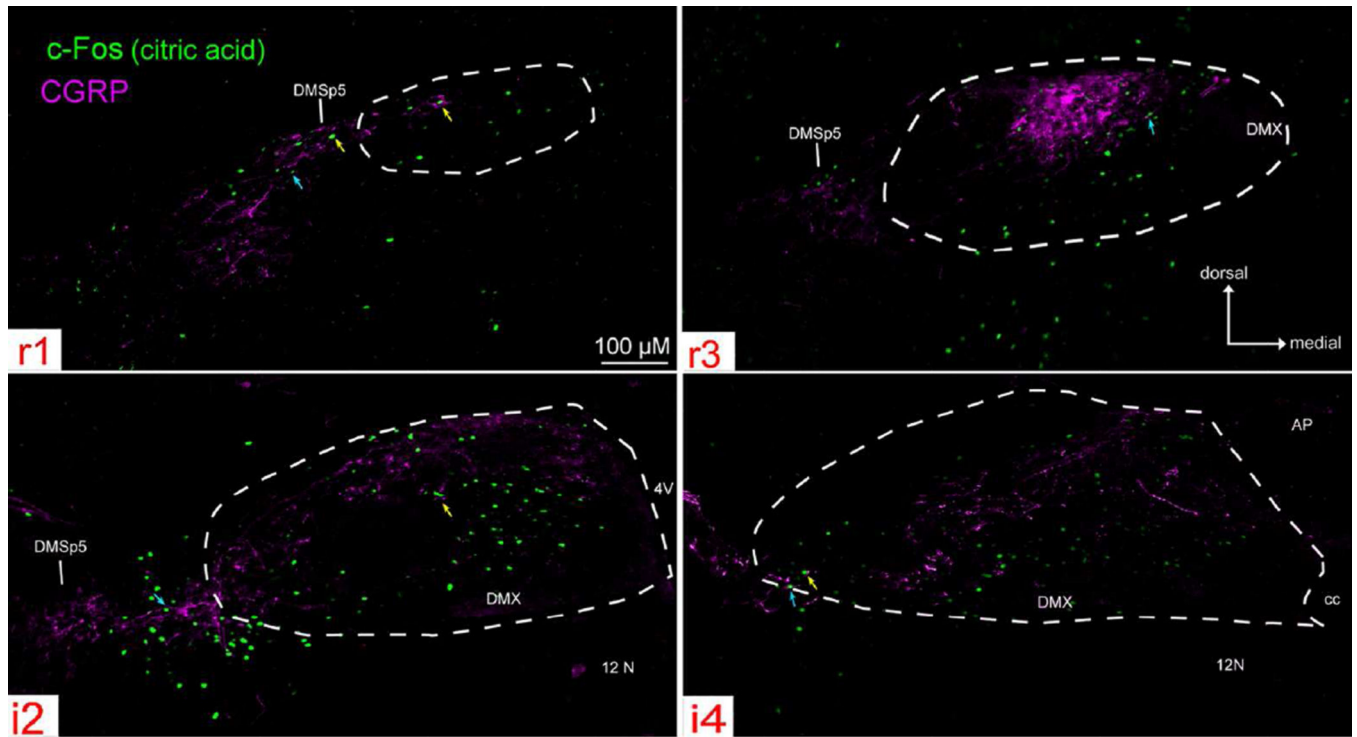


**Figure 10. Citric acid- evoked c-Fos-like Immunoreactivity (Fos-LI) within the brainstem of 'Control' (P2X WT) mice across four representative nTS levels (r1, r3, i2, i4)**  
 Photographs of citric acid-evoked c-Fos (green) and CGRP (magenta) staining, with nTS boundaries indicated as white dotted lines. Citric acid-evoked c-Fos positive cells lie primarily in areas that contain CGRP immunoreactive fibers (blue arrows) or terminals (yellow arrows).

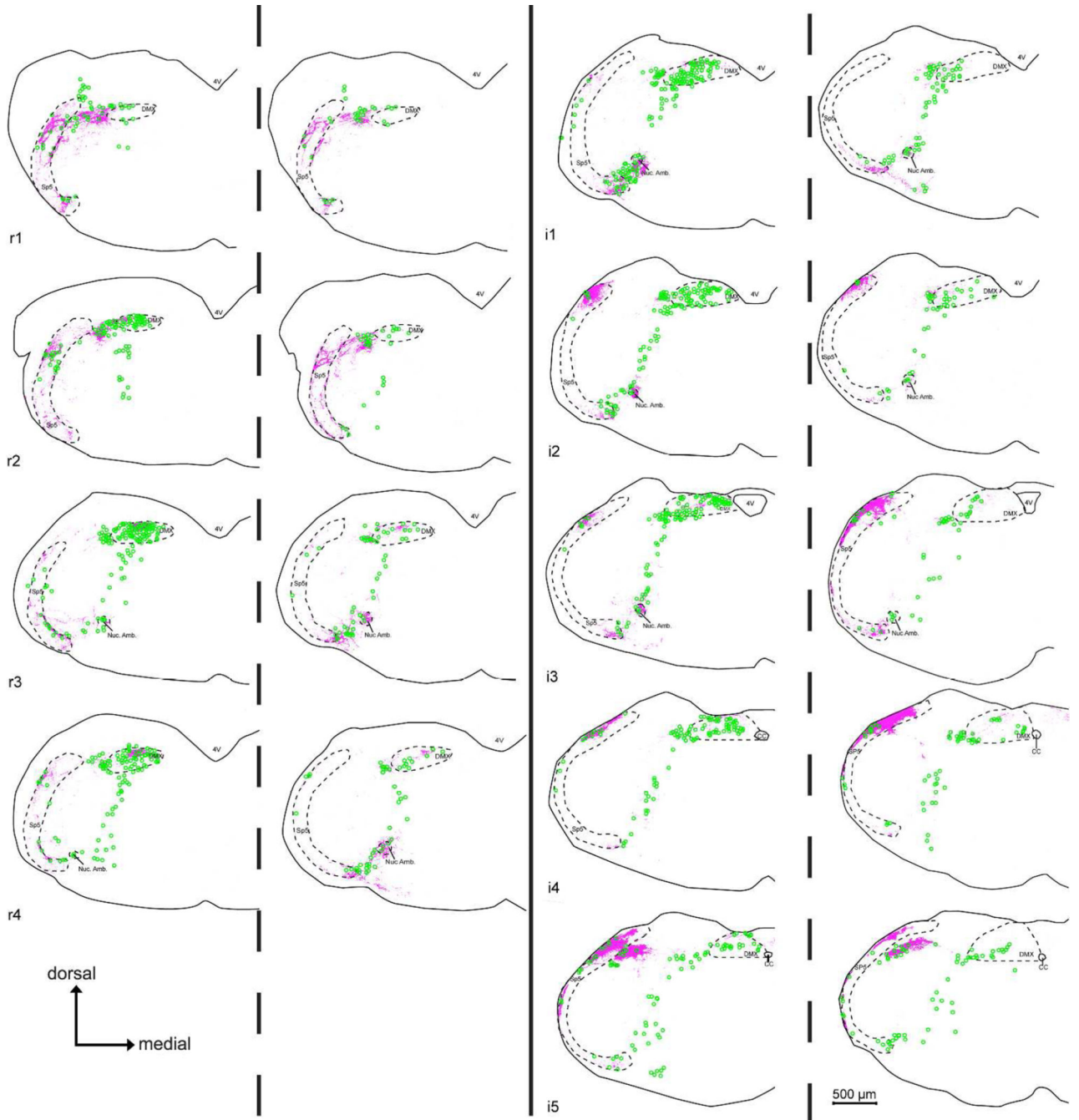
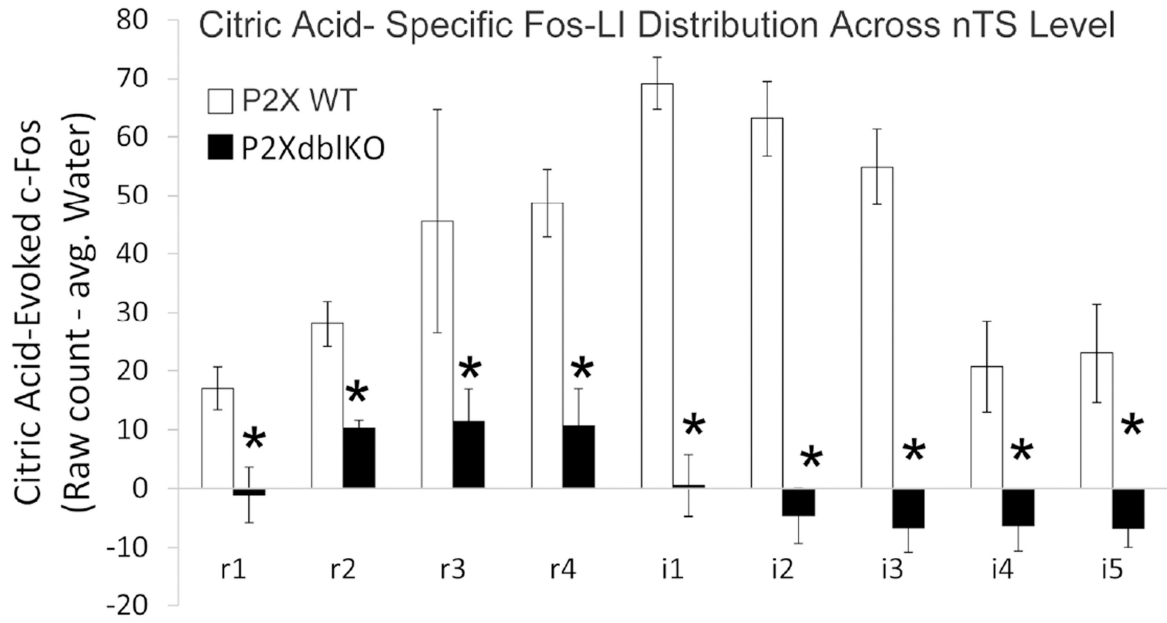


**Figure 11. Comparison chartings of citric acid-evoked c-Fos-like Immunoreactivity (Fos-LI) within the brainstem of 'Control' (P2X WT) (Left side of each pair) and 'Taste Blind' (P2X-dbl KO) (Right side of each charting pair) mice**

Across all nTS levels, Fos-LI (green circles) is significantly reduced in the nTS of P2X-dbl KO mice compared to WT. In contrast, in non-nTS areas displaying high levels of CGRP-immunoreactivity (magenta fibers), including the dorsomedial trigeminal nucleus (DMSp5), spinal trigeminal tract (SP5), and the nucleus Ambiguus (Nuc. Amb.), Fos-LI density is similar between P2X WT and P2X-dblKO mice.



**Citric Acid- Specific Fos-LI Distribution Across DMSp5 Level**

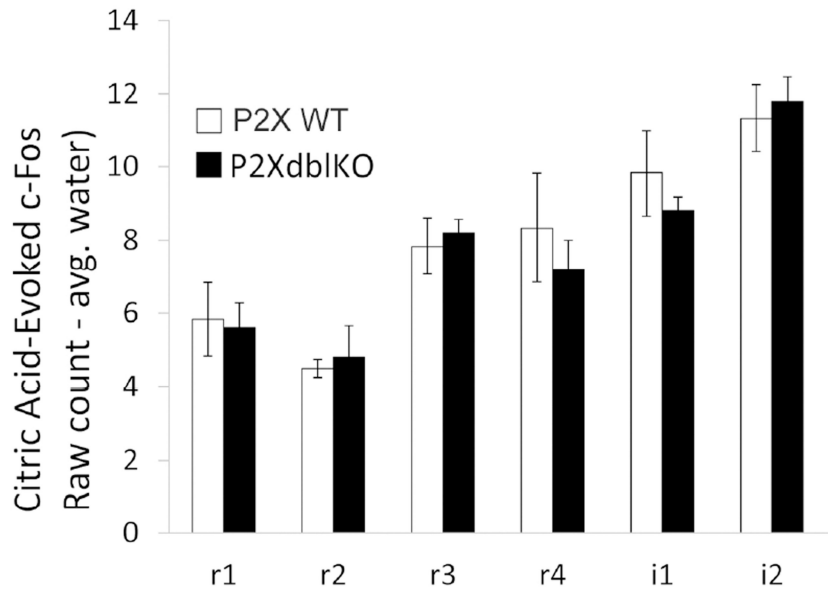


**Figure 12. Quantitative comparison of citric acid-evoked Fos-LI (raw count – avg. water) within the brainstem of P2X WT and P2X-dblKO mice across the different levels of the nTS and in the DMSp5**

**A.** The number of Fos-LI neurons is significantly reduced across all nTS levels in the nTS of P2X-dbl KO mice, (\* = Post hoc Tukey’s HSD results from main Group×nTS level ANOVA interaction is  $p < 0.05$ ). Note also the paucity of Fos-LI in P2X-dblKO mice in more caudal portions of the nTS (i4, i5) wherein esophageal afferents terminate. **B.** In contrast, Fos-LI is similar between P2X WT and P2X-dbl KO mice in the dorsomedial trigeminal nucleus (DMSp5).

		WT				P2X-dbl KO			
		nTS			DMSp5	nTS			DMSp5
		L	Mid	M		L	Mid	M	
r1	D	6.3	0.3	4.2	5.8	-2.4	1.7	-2.8	5.6
	V	0.3	3.7	2.2		1.8	0.3	0.3	
r2	D	7.0	9.8	3.7	4.5	3.9	3.8	2.6	4.8
	V	0.5	5.8	1.2		1.3	4.1	2.6	
r3	D	3.5	11.8	6.7	7.8	3.6	0.5	1.4	8.2
	V	6.2	14.3	3.0		-0.1	1.8	4.2	
r4	D	1.8	11.5	14.3	8.3	2.6	-5.7	2.4	7.2
	V	8.5	12.3	0.2		5.8	4.6	0.9	
i1	D	6.2	12.5	18.2	9.8	3.2	-5.1	-5.5	8.8
	V	18.2	11.8	2.3		6.6	-1.4	2.7	
i2	D	4.2	13.3	12.5	11.3	4.8	-1.1	-4.3	11.8
	V	26.2	13.2	-6.2		-2.6	-0.8	-0.6	
i3	D	6.0	15.8	8.0		-2.1	1.8	0.0	
	V	18.3	7.2	-0.5		-1.9	-4.5	0.1	
i4	D	-0.2	8.5	7.0		3.7	-2.5	-2.6	
	V	2.0	3.2	0.2		-2.6	-1.7	-0.6	
i5	D	4.5	5.5	-0.8		-2.7	-1.0	-3.8	
	V	2.8	8.2	2.8		1.9	1.2	-2.3	

**Figure 13. Spatial pattern ‘heat maps’ comparison of counts of citric acid- specific Fos-LI neurons within the brainstem of P2X WT and P2X-dblKO mice**

Left: citric acid- specific (raw count – avg. water) Fos-LI for P2X WT mice. Right: citric acid- specific (raw count – avg. water) Fos-LI for P2X-dblKO mice. Each 3×2 box within each major column represents one level of the nTS subdivided into the component subfields: lateral (L), Mid, medial (M) in dorsal (D) & ventral (V) tiers. Each heat map is color coded so that blue = minimal; red = maximal (> 15). For clarity, negative numbers (i.e. where citric acid Fos-LI was less than water-evoked Fos-LI) are shown as grey. All numbers represent the average value (n= 5 for P2X WT; n = 6 for P2X-dblKO) for each anatomical area (nTS subregion or DMSp5 region). In P2X WT animals, maximal activity in the Mid nTS levels r3 – i3 corresponds approximately to the RC subnucleus described by Ganchrow *et al.*, 2014. In P2X-dbl KO mice, citric acid-specific Fos-LI was substantially reduced in nearly all nTS areas, except the RL division, which receives a substantial trigeminal CGRP input. Similarly, no reduction in Fos-LI occurred in the DMSp5 which also receives trigeminal CGRP inputs.

**Table 1**

## Age and Sex of All Animals Used

Staining Combination	Mouse	Age (days)	Sex	Animal Identification
P2X2, ChAT-GFP, Nissl	ChAt-tauGFP	193	M	110705A
P2X2, ChAT-GFP, Nissl	ChAt-tauGFP	193	M	110705B
P2X2, ChAT-GFP, Nissl	ChAt-tauGFP	193	M	110705C
P2X2, NPY, Nissl	C57B16/J	111	M	110907B
P2X2, NPY, Nissl	C57B16/J	111	M	110907A
P2X2, NPY, Nissl	C57B16/J	124	M	110920A
P2X2, Galanin, Nissl	C57B16/J	180	F	110920D
P2X2, Galanin, Nissl	C57B16/J	156	M	110928A
P2X2, Galanin, Nissl	C57B16/J	156	M	110928B
NPY, Galanin, Nissl	C57B16/J	203	M	11109c
P2X2, CGRP, Nissl	C57B16/J	117	F	110928C
P2X2, CGRP, Nissl	C57B16/J	106	F	110928D
P2X2, CGRP, Nissl	C57B16/J	161	F	111027A
CGRP, Fluoromeylin	C57B16/J	180	F	110920C
Galanin, Fluoromeylin	C57B16/J	276	F	111027B
NPY, Fluoromeylin	C57B16/J	185	F	120823A
ChAT-GFP, Fluoromeylin	ChAt-tauGFP	88	F	130801A
Citric Acid-Evoked c-Fos/ CGRP	P2X WT	275	M	101021b
Citric Acid-Evoked c-Fos/ CGRP	P2X WT	247	M	110803
Citric Acid-Evoked c-Fos/ CGRP	P2X WT	291	F	120701b
Citric Acid-Evoked c-Fos/ CGRP	P2X WT	172	M	140929a
Citric Acid-Evoked c-Fos/ CGRP	P2X WT	186	M	141013
Citric Acid-Evoked c-Fos/ CGRP	P2X-dbl KO	190	F	141103
Citric Acid-Evoked c-Fos/ CGRP	P2X-dbl KO	296	M	100915b
Citric Acid-Evoked c-Fos/ CGRP	P2X-dbl KO	257	M	110701a
Citric Acid-Evoked c-Fos/ CGRP	P2X-dbl KO	263	F	110804
Citric Acid-Evoked c-Fos/ CGRP	P2X-dbl KO	170	M	140929b
Citric Acid-Evoked c-Fos/ CGRP	P2X-dbl KO	186	M	141010
Deionized Water-Evoked c-Fos/CGRP	P2XWT	220	F	10118b
Deionized Water-Evoked c-Fos/CGRP	P2XWT	187	M	091207
Deionized Water-Evoked c-Fos/CGRP	P2X-dbl KO	167	M	101022b
Deionized Water-Evoked c-Fos/CGRP	P2X-dbl KO	222	F	090825c

**Table 2**

## Primary Antibodies

Antibody (Antibody Registry ID)	Antigen (sequence)	Source (catalog #)	Working Dilution
Rabbit polyclonal anti-P2X2 (AB_2040054)	synthetic peptide to rat C' terminus (SQQDSTSTDPKGLAQL)	Alomone Labs, LTD Jerusalem (APR-003)	1:500
Rabbit polyclonal anti- Neuropeptide Y (NPY) (AB_572253)	Neuropeptide Y; coupled to bovine thyroglobulin (BTg) with glutaraldehyde	ImmunoStar Hudson, WI (22940)	1:500
Guinea Pig polyclonal anti- Galanin (AB_518351)	synthetic peptide to porcine (HGWTLNSAGYLLGPHAIN HRSFHDKYGLA)	Peninsula Laboratories, LLC San Carlos, CA (T-5036)	1:1500
Rabbit polyclonal anti- $\alpha$ -CGRP (AB_518147)	synthetic peptide to mouse/rat N' terminus (HSCNTATCVTHRLAGLLSRSG GVVKDNFVPTNVGSEAF)	Peninsula Laboratories, LLC San Carlos, CA (T-4032)	1:2500
Rabbit polyclonal anti-c-Fos (AB_2314042)	synthetic peptide to human 4-17 residues (SGFNADYEASSRC)	EMD Millipore Billerica, Massachusetts (PC38)	1:3000

**Table 3**

## List of Abbreviations

Abbreviation	Anatomical Structure
12n	hypoglossal nucleus
4V	4th ventricle
AP	area postrema
CC	central canal
Cu	cuneate nucleus
DCn	dorsal cochlear nucleus
DMSp5	dorsomedial nucleus of the descending trigeminal complex
DMX	dorsal motor nucleus of the vagus
Ecu	external cuneate
icp	inferior peduncle
M	medial subnucleus of the nucleus of the solitary tract
nTS	nucleus of the solitary tract
PC	parvicellular subnucleus of the nucleus of the solitary tract
RC	rostrocentral subnucleus of the nucleus of the solitary tract
RL	rostrolateral subnucleus of the nucleus of the solitary tract
Sol. Tract	solitary tract
sp5	spinal trigeminal tract
Sp5O	spinal trigeminal nucleus pars oralis
Sp5I	spinal trigeminal nucleus pars interpolaris
SP5C	spinal trigeminal nucleus pars caudalis